Engineering Structures 273 (2022) 114986

Contents lists available at ScienceDirect

Engineering Structures

journal homepage: www.elsevier.com/locate/engstruct

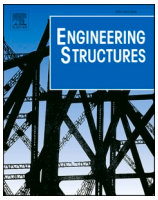

Investigations of the long-term extreme buffeting response of long-span bridges using importance sampling Monte Carlo simulations

Dario Fernandez Castellon [a,*], Aksel Fenerci [b], Ole Øiseth [a], Øyvind Wiig Petersen [a]

[a] Department of Structural Engineering, Norwegian University of Science and Technology, Richard Birkelands vei 1A, Trondheim, Norway
[b] Department of Ocean Operations and Civil Engineering, Norwegian University of Science and Technology, Larsgårdsvegen 2, 6025 Ålesund, Norway

ARTICLE INFO

Keywords:
Extreme buffeting response
Long-span bridge
Full long-term analysis
Monte Carlo simulations

ABSTRACT

Several studies have shown that site measurements of the buffeting responses of long-span bridges do not always agree with predictions from analytical models. The observed discrepancy is believed to be explained by the variability in the wind's turbulence field, which is ignored in the current design guidelines. Additionally, the guidelines neglect the true variability in the buffeting response, as this parameter is considered to be deterministically dependent on the mean wind speed only, and a single short-term-averaged wind condition is assumed to be representative of the bridge's behaviour over its lifetime. Such assumptions underestimate the design buffeting response. Alternatively, a full long-term analysis is regarded as the most accurate approach to handling extreme response estimations. Applications of this analysis in the wind engineering literature are scarce due to its large computational demand. With the objective of alleviating such demand, this paper proposes a full long-term analysis framework based on importance sampling Monte Carlo (ISMC) simulations and investigates, for the first time, the extreme buffeting response of a suspension bridge in its design phase with this framework. The results were compared with available formulations based on reliability methods and numerical integration. The proposed ISMC framework requires fewer simulations than the other formulations while maintaining a good degree of accuracy. The results show that the estimated extreme response is 30% larger than the current design guidelines suggest, showing the importance of considering the turbulence parameters' and loading effects' variabilities when calculating extreme responses.

1. Introduction

Determining the buffeting response is important for the structural design of long-span bridges under wind loads. Extensive research efforts have been pretended in the literature to enhance the understanding of this phenomenon. Experience with full-scale measurements and numerical simulations has shown that randomness in the wind's turbulence field has a strong effect on measured structural responses [1,2,11–13,3–10]. In particular, a study on the Hardanger Bridge concluded that the maximum buffeting response can occur for non-extreme wind speeds due to the higher significance of the variability in the wind's turbulence intensities [14]. Nevertheless, most of the current design guidelines for the structural design of long-span bridges assume the extreme buffeting response to be deterministically dependent on the extreme mean wind speed only [15]. Although mean wind speed is critical for the design and operation of long-span bridges [16,17], this approach not only neglects the variability in the wind's turbulence parameters and the buffeting response but also assumes that a single short-term-averaged wind condition is representative of the bridge's structural behaviour over its lifetime. Here, this approach is called the short-term method. Alternatively, a more accurate extreme response estimation may be found in the full long-term analysis (FLT). This strategy considers the variability in the loading effects and responses produced by changes in the weather conditions over the lifetime of a structure [18–20]. This methodology is a well-known standard for the structural design of offshore structures [21–28]. Studies conducted on the extreme buffeting response with the full long-term methodology have shown that the extreme response exceeded the estimations from the current design guidelines; therefore, it was concluded that the guidelines' assumptions may lead to the underestimation of the response [29,30]. Nevertheless, current literature confirming this statement is scarce, and hence, the motivation of this paper is to expand this knowledge.

* Corresponding author.
E-mail addresses: dario.r.f.castellon@ntnu.no (D. Fernandez Castellon), aksel.fenerci@ntnu.no (A. Fenerci), ole.oiseth@ntnu.no (O. Øiseth), oyvind.w.petersen@ntnu.no (Ø. Wiig Petersen).

https://doi.org/10.1016/j.engstruct.2022.114986
Received 18 February 2022; Received in revised form 6 September 2022; Accepted 17 September 2022
Available online 14 October 2022
0141-0296/© 2022 The Authors. Published by Elsevier Ltd. This is an open access article under the CC BY license (http://creativecommons.org/licenses/by/4.0/).

A crucial limitation that causes the full long-term methodology to be excluded from the wind engineering literature is its large computational demand. In this method, the estimation of the extreme response is a weighted average of the short-term response with the probability of the occurrence of each wind condition. This process involves the simulation of several wind conditions, making the method infeasible when multiple variables are considered. Several studies propose reducing the computational effort by reformulating the full long-term case as a reliability problem to be solved with inverse first- or second-order reliability methods (IFORMs or ISORMs) [19,30–32]. However, these methods converge to approximate solutions and struggle when the limit state function is highly nonlinear [33,34]. On the other hand, estimations of the long-term extreme response obtained through Monte Carlo simulations are recognized as being more robust than reliability methods [35–38]. The computational efficiency of Monte Carlo simulations can be improved by importance sampling Monte Carlo (ISMC) simulations, which simulate samples in the region that contributes most to the response evaluation [39]. For practical engineering applications, in which the extreme response must be calculated at several locations along the bridge, long-term analyses based on ISMC simulation promise to be more computationally efficient than those based on inverse reliability methods. Full long-term frameworks based on the ISMC approach have been reported in studies of offshore structures [36,38,40]. Nonetheless, the abovementioned studies focus on structures with design responses dominated by sea states, discounting the joint effect of the wind parameters that are relevant for long-span cable-supported bridges, such as the mean wind speed, turbulence intensities, turbulence spectral parameters, and turbulence coherence. Therefore, this paper proposes an investigation of the long-term extreme buffeting response of long-span bridges based on ISMC and considers uncertainties from multiple wind variables. The investigations are applied to the proposed Sulafjord Bridge in western Norway, a 2800 m single-span suspension bridge currently in the phase of design feasibility assessment, making this paper the first study to apply full long-term analysis in the early stage of the design of a long-span bridge.

The objectives of this study are twofold. First, we compare the extreme buffeting responses estimated with the short-term and long-term methodologies. Second, we propose a framework of full long-term extreme buffeting response estimation based on importance sampling, which promises to significantly reduce the computational effort of the full long-term analysis without the downside of converging to an approximate solution. Achieving these objectives requires the evaluation of 5 different computational models of extreme buffeting response estimation: 1) the short-term method used as the basis of the current design guidelines; 2) the environmental contour method (EMC); 3) the full long-term framework based on the numerical integration of weighted averaging; 4) the full long-term framework based on the IFORM; and 5) the proposed framework based on importance sampling. Notably, the scope of this study is the development of the framework itself rather than the full description of the structural responses of the Sulafjord Bridge and that wind-induced effects different than buffeting action are outside the scope of this paper.

The content of the paper is organized as follows: Section 2 summarizes the methods for extreme buffeting response estimations for long-span bridges and presents the proposed framework based on ISMC. Section 3 describes the Sulafjord site and the wind probabilistic model applicable to the design of the Sulafjord Bridge [41]. Section 4 describes the finite element model of the Sulafjord Bridge and the parameters required for the buffeting response formulation. Section 5 shows the investigations of the long-term extreme response of the Sulafjord Bridge computed with the five methods mentioned above, using the bending and torsional moments at the quarter-span of the bridge as the target metrics.

2. Long-term extreme buffeting response formulations

2.1. Extreme response obtained by the short-term method

The short-term method is a common approach used in most of the current design guidelines for wind-resistant design [15,42]. This approach defines the design buffeting response based on the extreme mean wind speed with a return period RP (equal to the structure's lifetime), which is averaged from periods of short-term duration (T_{st}). Such a wind condition will be denoted with $\boldsymbol{w}_{RP}$. During each short-term averaging period, the buffeting response (R) is assumed to be a stationary and Gaussian random process. The average upcrossing rate of a response value r during a period T_{st} is defined with the Rice formulation [43,44]:

$$V_R^+(r|\boldsymbol{w}_{RP}) = \frac{1}{2\pi}\frac{\sigma_{\dot{R}}(\boldsymbol{w}_{RP})}{\sigma_R(\boldsymbol{w}_{RP})} exp\left\{ -\frac{1}{2}\left(\frac{r-\mu_R(\boldsymbol{w}_{RP})}{\sigma_R(\boldsymbol{w}_{RP})}\right)^2 \right\} \tag{1}$$

where μ_R *and* σ_R are the mean and standard deviation of the buffeting response from buffeting theory and $\dot{x}$ denotes the time derivative of x. The statistical moments of the response and its time derivative process are found by integrating the response spectrum S_R as follows:

$$\sigma_R^2(\boldsymbol{w}_{RP}) = \int_0^\infty S_R(\boldsymbol{w}_{RP})d\omega$$

$$\sigma_{\dot{R}}^2(\boldsymbol{w}_{RP}) = \int_0^\infty \omega^2 S_R(\boldsymbol{w}_{RP})d\omega \tag{2}$$

Considering the upcrossings of large values of r as independent and rare events, it is possible to assume the probability of upcrossing large values of r during T_{st} as Poisson-distributed. In such a case, the probability of obtaining exactly n upcrossings is $\exp\{-V_R^+(r|\boldsymbol{w}_{RP})T_{ST}\}\frac{R^n}{n!}$., and the probability of obtaining no upcrossings ($n = 0$) is equal to the probability of $R \geq r$. Then, the cumulative distribution function of the largest values of R yields:

$$F_R(r|\boldsymbol{w}_{RP}) = exp\{-V_R^+(r|\boldsymbol{w}_{RP})T_{ST}\} \tag{3}$$

F_R is narrow for large responses. Davenport et al. (1964) suggested that it is sufficient to assume the largest response (R_{RP}) as the expected value of F_R[39] :

$$E[F_R(r|\boldsymbol{w}_{RP})] = \int_{-\infty}^{+\infty} r\frac{dF_R(r|\boldsymbol{w}_{RP})}{dr}dr \tag{4}$$

2.2. Extreme response through long-term formulations

2.2.1. Full long-term methodology

In contrast to the short-term method, the full long-term analysis considers the changes in weather conditions and their effect on the buffeting response over the lifetime of the bridge. Therefore, this methodology provides a more accurate estimation of the extreme buffeting response. Naess and Moan (2012) reported three different full long-term formulations: that based on the short-term peak distribution, that based on all short-term extremes, and that based on the upcrossing rate response [18–20,48]. These methods have been proven to be equivalent [40]. In particular, the method based on the upcrossing rate considers the average of the upcrossing rate V_R^+ and the joint probability of the wind variables f_W, yielding the following modification of Eq. (3):

$$Prob\{R_{RP}(T_{LT}) \leq r\} = F_{r_{RP}(T_{LT})}(r) = exp\{-V_R^+(r|\boldsymbol{w})T_{LT}\} \tag{6}$$

$$F_{R_{RP}(T_{LT})}(r) = \exp\left\{ -T_{LT}\int_W V_R^+(r|w)f_W(w)dw \right\}$$

where $\boldsymbol{W} = \{VI_u I_w A_u A_w K_u K_w\}$ is the vector containing the stochastic wind parameters, such as the mean wind speed, the along-wind and

vertical components of the turbulence intensity, the spectral parameter and the decay coefficient. Further details of these parameters are provided in section 3.1.1. $V_R^+(r|\boldsymbol{w})$ is the short-term average of the upcrossing of the response level r given the wind condition $\boldsymbol{w}$.

Solving Eq. (6) involves numerical integration, which in general demands a large computational effort that increases with the number of wind variables considered. Hence, the motivation in the wind engineering and structural reliability literature is to implement an alternative solution that can be both fast and accurate. As this approach tends towards an exact solution of the extreme response Eq. (6) will be regarded as the exact formulation of the full long-term methodology throughout this paper.

2.2.2. Long-term formulation based on reliability methods

Giske et al. reformulated the exact formulation of the full long-term methodology as a reliability problem [19,31]. This formulation introduces an augmented vector of variables $\boldsymbol{Y}$ that incorporates the wind variable $\boldsymbol{W}$ and the approximated extreme response $\widetilde{R}_{RP}$.

$$\boldsymbol{Y} = [\boldsymbol{W}, \widetilde{R}_{RP}] \tag{7}$$

$$f_Y(y) = f_{\widetilde{R}_{RP}|W}(\widetilde{r}|\boldsymbol{w}) f_W(\boldsymbol{w})$$

The limit condition is established as a state of the variable $\boldsymbol{Y}$ that exceeds the actual extreme structural response $G(\boldsymbol{y}) = R(\boldsymbol{y}) - \widetilde{R}_{RP}$. Then, Eq. (6) is rewritten as:

$$\widetilde{F}_{R_{RP}}(r) = \int_{\widetilde{R}_{RP} \le r} f_Y(y)dy = 1 - \int_{G(y)\le 0} f_Y(y)dy = 1 - p_f \tag{8}$$

Here, p_f is the exceedance probability associated with RP and is a known quantity for reliability-based design. The maximum structural response is left as the unknown variable that is to be found with an inverse reliability method such as the IFORM [49]. The method works by transforming the variable set $\boldsymbol{Y}$ into a set of independent standard normally distributed variables $\boldsymbol{U}(u_1, u_2, \cdots, u_N)$ with the Rosenblatt transformation rule [50] (Appendix). In the space of the new set of variables, the reliability index β corresponds to the failure probability obtained through the joint standard normal cumulative distribution function $\Phi(\boldsymbol{x})$. The extreme response estimation is given by the optimization procedure below applied to Eq. (8). A detailed explanation of the procedure and formulation may be found in [22,31].

Given β, find $\widetilde{R}_{RP} = max|r(\boldsymbol{U})|; subject\ to |\boldsymbol{U}| = \beta$ (9).

$$p_f \cong \Phi(-\beta)$$

$$\beta \cong -\Phi^{-1}(p_f) \tag{10}$$

2.3. Long-term formulation based on importance sampling

The full long-term framework based on the IFORM converges to an approximate solution, and the accuracy of the method is challenged when the limit state function is highly nonlinear or when multiple limit states are considered. Monte Carlo simulations bypass these limitations by evaluating the short-term responses for simulated wind states and reformulating the average of Eq. (6) as a statistical average that converges to the exact solution:

$$F_{R_{RP}(T_{LT})}(r) = exp\left\{ -\frac{T_{LT}}{N_{sim}} \sum_{i=1}^{N_{sim}} V_R^+(r|\boldsymbol{w}_i) \right\} \tag{11}$$

where N_{sim} is the number of simulations to be checked with the convergence criterion.

The crude Monte Carlo method of Eq. (11) may converge slowly and hence motivate the implementation of an importance sampling strategy [39]. This approach works by generating the wind states from the sampling function h_W, which is located in the region that overlaps the maximum values of the short-term buffeting response with the joint probability of the wind variables. Since the derivation of an optimal sampling function is a cumbersome procedure outside the scope of this study, the location of the sampling is determined a priori from engineering experience. With the new sampling function, Eq. (11) now becomes:

$$F_{R_{RP}(T_{LT})}(r) = exp\left\{ -\frac{T_{LT}}{N_{sim}} \sum_{i=1}^{N_{sim}} V_R^+(r|\boldsymbol{w}_i) \frac{f_W(\boldsymbol{w}_i)}{h_W(\boldsymbol{w}_i)} \right\} \tag{12}$$

The simulation scheme is further simplified by generating the samples as independent standard normally distributed variables, $\boldsymbol{U}$, which are then transformed into wind state variables through the Rosenblatt transformation rule [50] (Appendix A). Then, Eq. (12) is performed over the transformed set of variables:

$$F_{R_{RP}(T_{LT})}(r) = exp\left\{ -\frac{T_{LT}}{N_{sim}} \sum_{i=1}^{N_{sim}} V_R^+(r|\boldsymbol{u}_i) \frac{f_U(\boldsymbol{u}_i)}{h_U(\boldsymbol{u}_i)} \right\} \tag{13}$$

It is common practice to use a normal distribution as a sampling function. This is, however, not feasible in this case since it will produce extremely high wind velocities for which the buffeting response model used in this paper will yield inaccurate results. Therefore, a uniform distribution is used since this represents the simplest possible alternative. Then, the sampling function is chosen as an N-sized multiple uncorrelated uniform distribution:

$$h_U(\boldsymbol{u}) = \prod_{k=1}^{N} \mathscr{U}_k(x|a_k, b_k) \tag{14}$$

where $k = \{1, 2, \cdots, N\}$ is an index of the stochastic variables and $\mathscr{U}(a, b)$ is the uniform distribution with lower and upper limits a and b:

$$\mathscr{U}(x) = \begin{cases} \dfrac{1}{b-a}, for x \in [a, b] \\ 0 \quad , elsewhere \end{cases} \tag{15}$$

The distribution limits a *and* b are chosen such that the generated wind states are within the domain in which the response prediction model is accurate.

3. Long-term investigations of the Sulafjord bridge

Investigations of the long-term buffeting response of the Sulafjord Bridge were chosen as a case study. A description of the bridge site and its wind conditions are presented in the next section.

3.1. Site-specific wind characterization

Fig. 1 shows the Sulafjord site and its surroundings. The fjord is in the vicinity of Ålesund city in western Norway. Castellon et al. [41] developed a probabilistic model of the wind variability at the site based on the data from site measurements and hindcast mesoscale simulations [51–53]. Wind measurement data were collected by the Norwegian Meteorological Institute [54]. The wind measurements were carried out at four mast stations equipped with WindMaster Pro 3-Axis anemometers (Gill Instruments Limited) (Max speed: 65 m/s; Resolution: 0.01 m/s 0.1°; Accuracy: less than1.5 % RMS at 12 m/s and 2°).

The mast measurement stations are symbolized with crosses in Fig. 1. The hindcast data were collected at those same locations and at an additional point at the centre of Sulafjord, represented by a circle in Fig. 1. The proposed location for a suspension bridge is shown with a thick line in Fig. 1. Castellon et al. (2022) suggested that the Sulafjord centre and Trælboneset station are the locations with the closest expected behaviour compared to the bridge track. Therefore, their data were used to establish the probabilistic modelling [41]. Finally, Fig. 2 shows an illustration of the Sulafjord suspension bridge adapted from

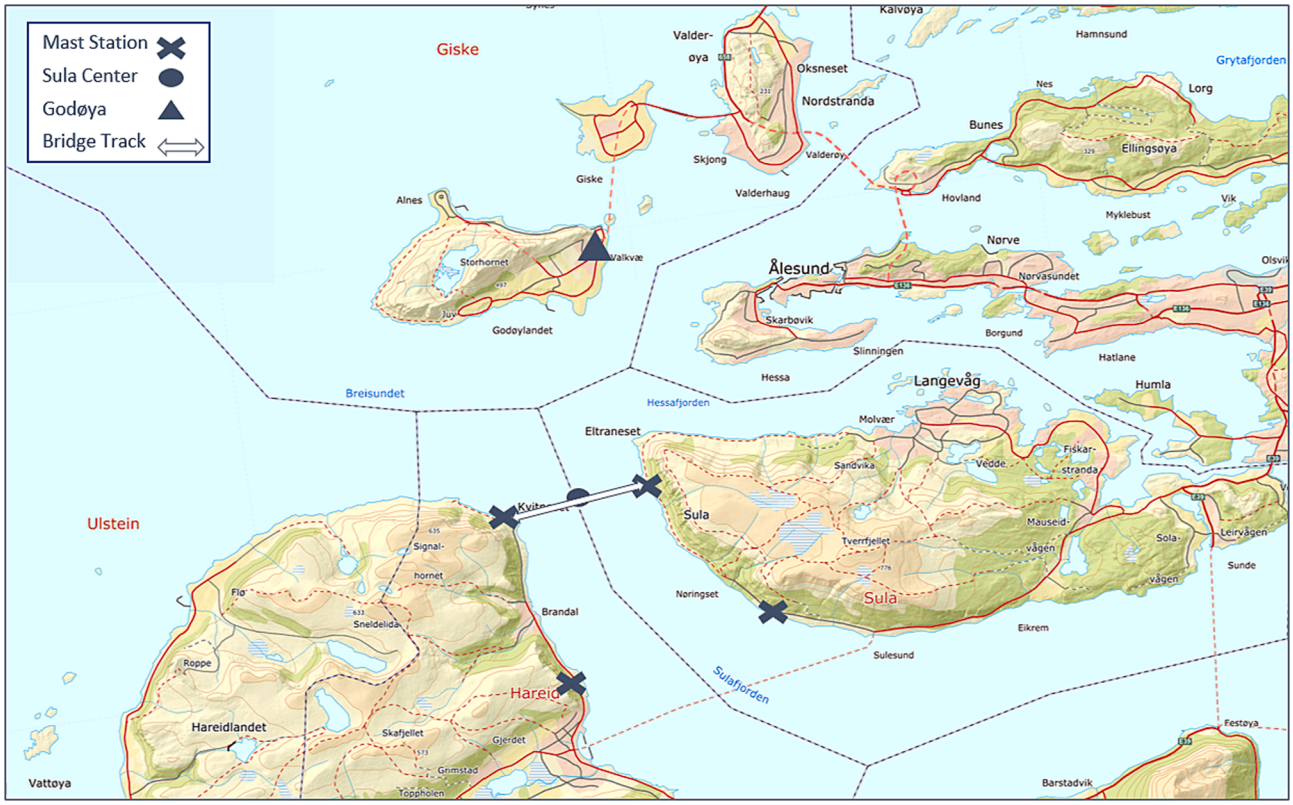

Fig. 1. Topographical map of the Sulafjord site (adapted from https://norgeskart.no/- ®norgeskart Norwegian Mapping Authority).

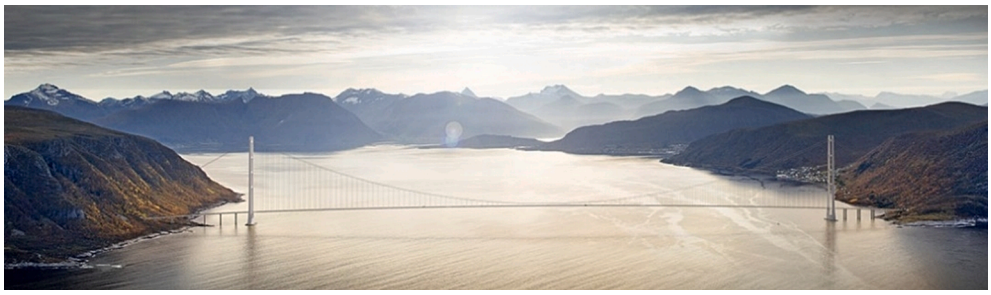

Fig. 2. Illustration of the Sulafjord suspension bridge (image courtesy of NPRA).

studies by the Norwegian Public Roads Administration (NPRA) [55]. Further details about the wind measurement and the bridge site may be found in [10 41].

3.1.1. Turbulence parameters

The turbulence was modelled from its cross-spectrum S_{nn}, where the one-point spectrum S_n was considered a Kaimal type and the spatial coherence Coh_n was taken as exponential decay with Davenport's coefficients [56,57]. Model uncertainties were introduced by assuming the mean wind speed (V), along-wind and vertical turbulence intensities (I_u, I_w), spectral parameters (A_u, A_w) and decay coefficients (K_u, K_w) as stochastic variables. Cross-wind turbulence parameters and 3-dimensional coherence were not considered in this analysis because of their small contribution to the overall buffeting response of the bridge.

$$\frac{S_n f}{(VI_n)^2} = \frac{A_n f_{z_h}}{\left(1 + 1.5A_n f_{z_h}\right)^{5/3}}, f_z = \frac{z_h f}{V}, I_n = \frac{\sigma_n}{V}$$

$$Coh_n(f, \Delta x) = exp\left(-K_n \frac{\Delta x f}{V}\right) \tag{16}$$

$$S_{nn}(f, \Delta x) = Coh_n(f, \Delta x)\sqrt{S_n(x_i)S_n(x_j)}$$

The subscripts $n \in \{u, w\}$ indicate the along-wind and vertical turbulence components, z_h is the reference height, and f is the frequency. σ_n represents the standard deviation, and Δx is the distance between two wind nodes.

3.2. Probabilistic wind field model

In this paper, we used the probabilistic model of the wind field at the Sulafjord site reported in Castellon et al. [41]. The following section introduces the key aspect of the probabilistic model; for further details, please refer to [41].

3.2.1. Mean wind speed

Full long-term analysis requires the simulation of several wind states, most of which have a relatively low mean wind speed but a high probability of occurrence. A Weibull (parent) distribution is suitable for describing such wind states. The shape of the Weibull distribution is as follows:

$$F_V(V) = 1 - exp\left[\left(\frac{V}{\lambda}\right)^k\right]; for V > 0 \quad (17)$$

where F_V is the cumulative density function (CDF) of the mean wind speed using a 10-minute averaging period and k *and* λ are the shape and scale distribution parameters, respectively.

Establishing the parent distribution from the mean wind speed data may not provide a satisfactory description for strong wind speeds in the upper tail region. Hence, using the method of the independent storms, we established the distribution parameters equivalent to a type 1 generalized extreme value distribution (Gumbel) from the annual largest mean wind speeds reported in the hindcast simulation at the Sulafjord centre. This technique reinforced the establishment of the distribution towards the strong mean wind speeds. A detailed explanation of the procedure is given in [41]. Table 1 presents the values of the distribution parameters adopted from the Sulafjord characterization reported in [41]. Table 2 shows the mean wind speeds for 50-, 100-, and 500-year return periods.

3.2.2. Wind turbulence parameters

The turbulence parameters, namely, turbulence intensities (I_u, I_w), spectral parameters (A_u, A_w) and decay coefficients (K_u, K_w), were established as joint lognormal distributions conditional on the mean wind speed and direction. The distribution values for the spectral parameters and the turbulence intensities were adopted from the mast measurement data recorded at Trælbonset station, as explained in [41]. However, the long distance between the stations in the mast measurement campaign weakens the validity of the distribution parameters for the decay coefficients. Therefore, the values of K_u and K_w were adopted from the probabilistic model of the Hardanger Bridge based on full-scale measurements [58]. Table 3 and Table 4 report the distribution parameters conditional on the mean wind speed and the correlation coefficient matrix, respectively.

4. Sulafjord bridge modelling and buffeting response

This section shows an overview of the modelling and the structural parameters involved in the buffeting response predictions. The buffeting response over the short-term averaging period was computed with multimode theory [59–61]. The computational formulation used for introducing the aerodynamic loads in the finite element model is described in [62]. Refer to the abovementioned references for further details. The buffeting response is computed in the frequency domain, yielding the cross-spectrum of any required response parameter S_R.

4.1. Finite element model

The modal properties of the Sulafjord Bridge were obtained from a finite element model developed in Abaqus 2019 software [63]. The model shown in Fig. 3 is a spine-beam model in which each of the girders is modelled with Timoshenko beam elements. The distance between the hangers is 24 m. The main cable is modelled by Timoshenko beam elements with an area of 0.6 m^2. The cross-sectional properties of the components are reported in Table 5, and the twin deck configuration is illustrated in Fig. 4. To increase the stability limit of the bridge, a central buckle is added in the midspan. This is modelled as a pretensioned cable connection between the main suspension cables and the bridge deck (Fig. 5) that restricts the relative lateral displacement between the two. In this way, the frequency of the first antisymmetric torsional mode is increased, and the stability of the bridge is enhanced [64]. Similar types of mechanical restraints have been used in other long-span bridges, such as the Great Belt Bridge and the Akashi Kaikyo Bridge.

The nonlinear behaviour of the cable is considered in the application of the dead loads. Subsequently, a modal analysis is performed with the linearized geometric stiffness of the completed state of the bridge, and it is solved for the first 100 modes in a frequency range of 0.03 to 0.66 Hz. The structural damping for still-air conditions is assumed to be proportional modal damping with a critical damping ratio coefficient $\zeta = 0.005$ for all modes. The mode shapes of the first 6 modes in the still-air condition are illustrated in Fig. 6, and Table 6 reports the natural frequencies up to the 15th mode.

Table 1
Parameters of the parent distributions from the measured data.

Location	Direction	λ	k
Sulafjord-centre	South	1.52	0.82

Table 2
Mean wind speeds in [m/s] for different return periods.

Location	V_{50}	V_{100}	V_{500}
Sulafjord centre	39.83	42.10	47.46

Table 3
Statistical parameters of the turbulence model.

	$\widetilde{\mu}$	$\widetilde{\sigma}$
I_u	$-2.381 - 0.003V$	0.206
I_w	$-2.588 - 0.015V$	0.208
A_u	2.054	0.855
A_w	1.314	0.800
K_u	2.109	0.268
K_w	2.163	0.332

Table 4
Correlation coefficient fit matrix of the turbulence model.

	I_u	I_w	A_u	A_w	K_u	K_w
I_u	1.00					
I_w	0.67	1.00		Symmetric		
A_u	0.00	0.00	1.00			
A_w	0.00	0.47	0.00	1.00		
K_u	0.00	0.00	0.00	0.00	1.00	
K_w	0.00	0.00	0.00	0.00	0.47	1.00

4.2. Dampers to enhance the flutter stability limit

Flutter stability is a critical phenomenon for long-span bridges. To enhance the stability flutter limit for the bridge design under consideration, 4 tuned passive damping devices were added. The devices were modelled as pairs of linear spring and damper elements connected between the main cable of the bridge and the support towers. The effect of the damping system in the bridge's finite element model was considered with additional stiffness and damping matrices from the devices ($\boldsymbol{C}_d, \boldsymbol{K}_d$) [64]:

$$C_d = \sum_j c_j w_j w_j^T, K_d = \sum_j k_j w_j w_j^T \quad (18)$$

where $\boldsymbol{w}_j$ is the connectivity vector of the device, j is the device damping, and c_j and k_j are the stiffness parameters. The damping system is tuned to subtract energy from the lowest vertical and torsional modes so that the flutter instability is reduced. The procedure starts by defining the device's location and connectivity $\mathbf{w}_j$, followed by Bayesian optimization of the parameters c_j and k_j to maximize the critical velocity for flutter instability. The optimization was performed with the bayesopt function in MATLAB [65], by optimizing c_j from 1e + 06 to 1e + 08 and k_j from 5e + 05 to 1e + 07, the limits defined by the appropriate engineering criterion. The tuned parameters are reported in Table 7. The addition of the damping devices increased the critical velocity from 60.3 m/s to 67.2 m/s.

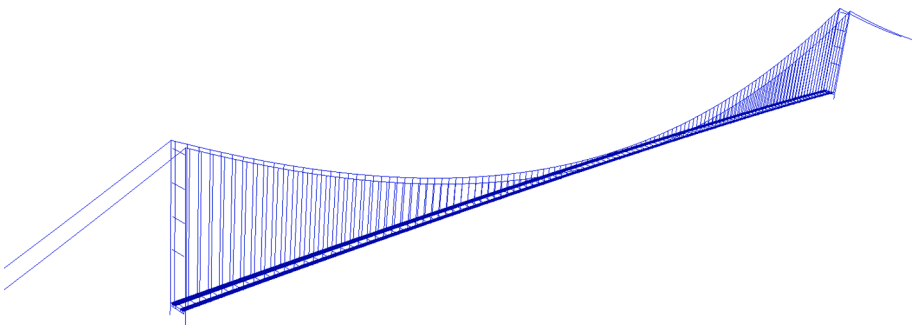

Fig. 3. Finite element model of the Sulafjord Bridge.

Table 5
Cross-sectional properties of the structural components in the model: The properties of the girder are reported for a single bridge deck at its local centre of area.

	Area $[m^2]$	Second moment of area Weak axis $[m^4]$	Second moment of area Strong axis $[m^4]$	Torsional constant $[m^4]$	Young modulus $[N/m^2]$	Shear modulus $[N/m^2]$
Girder	0.732	0.64	17.14	1.852	2.1e + 11	8.00e + 10
Hanger	0.0040	1.0e-07	1.0e-07	1.0e-07	1.6e + 11	6.15e + 10
Cable	0.6	2.86e-04	2.86e-04	5.73e-04	2.0e + 11	7.69e + 10

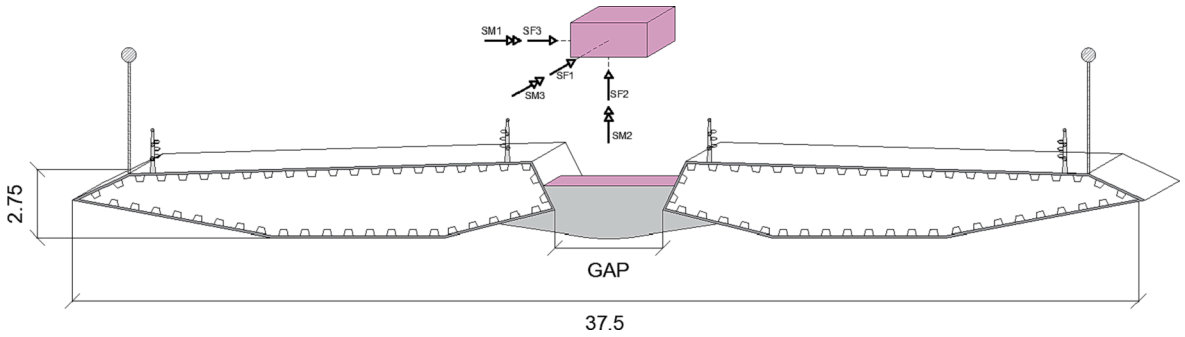

Fig. 4. Twin deck cross-section of the Sulafjord Bridge (units are in metres).

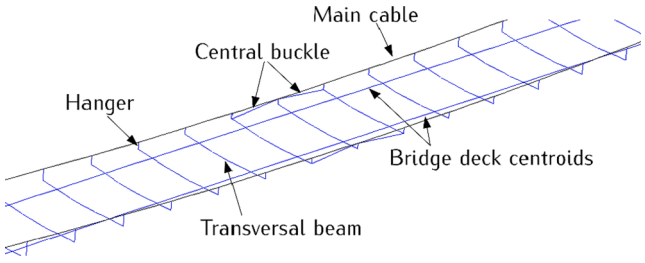

Fig. 5. Components of the finite element model at the midspan location.

4.3. Wind tunnel test results

Wind tunnel testing of the cross-section for the Sulafjord Bridge was carried out at the Norwegian University of Science and Technology (NTNU) laboratories using a state-of-the-art forced vibration method for motion with three degrees of freedom [66]. Fig. 7 a) shows the axis of the buffeting actions and force coefficients, and Figure b) shows the static force coefficients versus the angle of attack and their linearization around zero degrees. In Fig. 7, $\overline{V}$ represents the mean wind velocity vector, and the components u, v and w are the along-wind, cross-wind and vertical turbulence components, respectively. The values of the coefficients and their derivatives in the zero-degree linearization point are reported in Table 8.

Aerodynamic derivatives and admittance functions influence the structural response while exhibiting stochastic behaviour. However, including these parameters in probabilistic modelling requires the collection of a sufficiently large database from wind tunnel testing of the Sulafjord Bridge. As such database is not yet available, these parameters were adapted from the experimental data in a deterministic manner. Fig. 8 and Fig. 9 show the experimental results of the 18 aerodynamic derivatives, as well as polynomial functions that are fitted to the scattered data. Constant values are used outside the range of available experimental data. In the figures, the reduced (nondimensional) frequency $K = \frac{\omega B}{V}$ is used in the abscissa, as is common for wind tunnel test data.

5. Results & discussion

This article focuses on the development of the full long-term analysis framework and providing the actual structural responses of the Sulafjord Bridge is outside of the scope of work. The framework is applicable to any response component. Therefore, in this study the displacement responses of the Sulafjord bridge in the lateral and vertical direction (R_y, R_z), as well as rotation around the longitudinal axis (R_t torsion) were included to exemplify the methodology. While the structural weak- and strong-axis bending moments (SM1 and SM2) and the torsional moment (SM3) were chosen to verify in detail the features of the methodology. The following section shows the results and comparison from the different analyses.

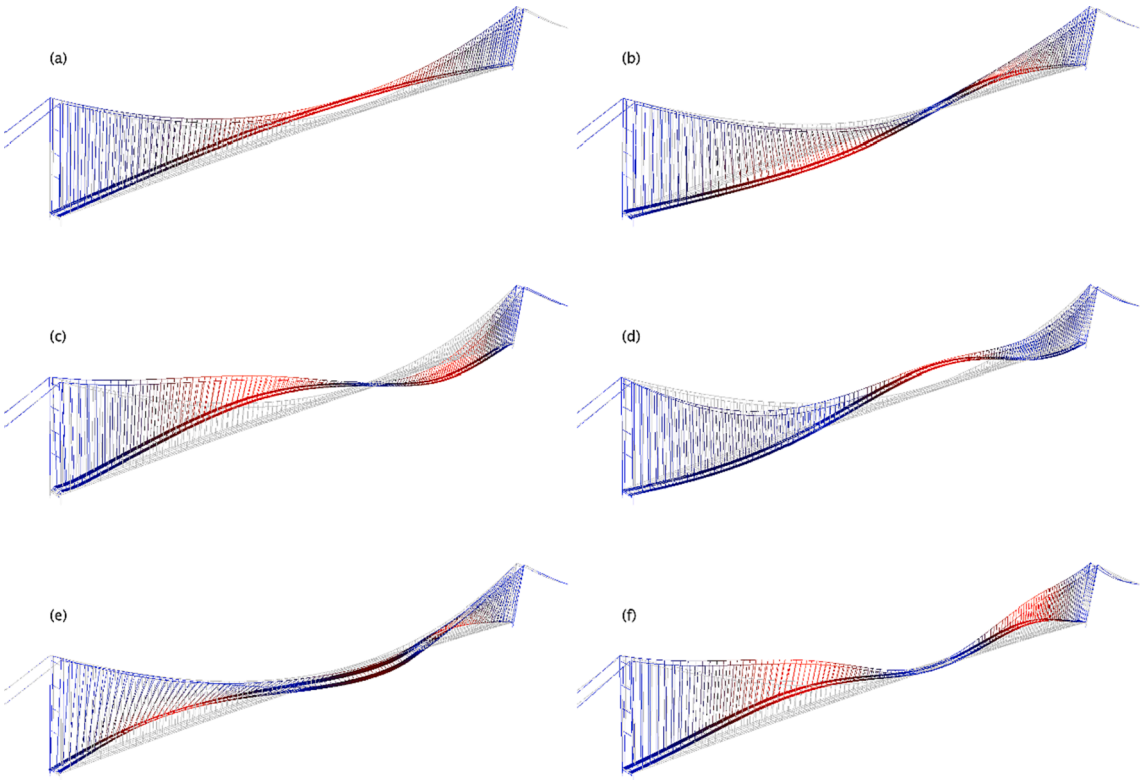

Fig. 6. Mode shapes of the six lowest vibration modes of the bridge.

Table 6
Natural frequencies of the still-air modes.

Mode	Frequency [Hz]	Circular Frequency [rad/s]	Label	Characteristic
1	0.0317	0.199	H1	Horizontal girder
2	0.0655	0.411	H2	Horizontal girder
3	0.0797	0.501	V1	Vertical girder
4	0.0839	0.527	V2	Vertical girder
5	0.1078	0.678	H3	Horizontal girder
6	0.1140	0.716	V3	Vertical girder
7	0.1252	0.786	V4	Vertical girder
8	0.1276	0.802	T1	Torsional girder
9	0.1307	0.821	T2	Torsional girder
10	0.1358	0.853	CH1	Horizontal cable
11	0.1372	0.862	CH2	Horizontal cable
12	0.1382	0.868	CH3	Horizontal cable
13	0.1413	0.888	CH4	Torsional girder
14	0.1578	0.992	V5	Vertical girder
15	0. 1628	1.023	H4	Horizontal girder

Table 7
Tuned damper parameters.

c_j [kg/s]	k_j [N/m]	$V_{critical}$ [m/s]
2.32e + 06	9.08e + 05	67.2

5.1. Buffeting response according to the short-term design method

In what follows, the extreme buffeting response from the short-term method is compared with the long-term estimations to check whether the 30 % difference between the approaches observed in the Hardanger Bridge case study [34] is also present for the Sulafjord Bridge. The return period of the investigations is set to 100 years, as this is the usual operational lifetime of long-span bridges. This chapter explores the features of the buffeting response for short-term estimation.

5.1.1. Short-term buffeting response

The extreme mean wind speed for the 100-year return period is reported in Table 2. The current dominating method in the design guidelines is to establish the wind turbulence parameters from a deterministic relation to the extreme mean wind speed. Therefore, the turbulence parameters for the short-term method were chosen as the most likely values from their marginal distributions conditioned on the mean wind speed. The distribution parameters are reported in Table 3. Table 9 reports the wind state used for the short-term estimation.

The responses components investigated were located at the quarter span of the Sulafjord bridge. Fig. 10 shows the mean value of the responses along the longitudinal axis of girder 1, and Fig. 11 shows the standard deviations (see the force notation in Fig. 4). The influence of the hanger insertion points on the girder can be seen as evenly spaced crests in the figures, whereas the peaks close to the midspan are force concentrations due to the central buckle. The statistical properties of the buffeting response are summarized in Table 10.

The extreme buffeting response from the short-term method was obtained from Eq. (4). The resulting responses are reported in Table 11. Extreme responses in the table and subsequent calculation do not include the mean response value.

5.1.2. Extreme response based on environmental contours

As an alternative to the design wind speed, the short-term extreme response could be found for all the points along the environmental contours of the wind variables. The extreme response corresponds to the maximum peak response along the contour. The contours of the wind variables at the Sulafjord Bridge location are reported in [41]. Table 12 reports the wind design conditions and the extreme buffeting response with the ECM. The extreme buffeting responses from the ECM are higher than those from the short-term method. The difference is due to the

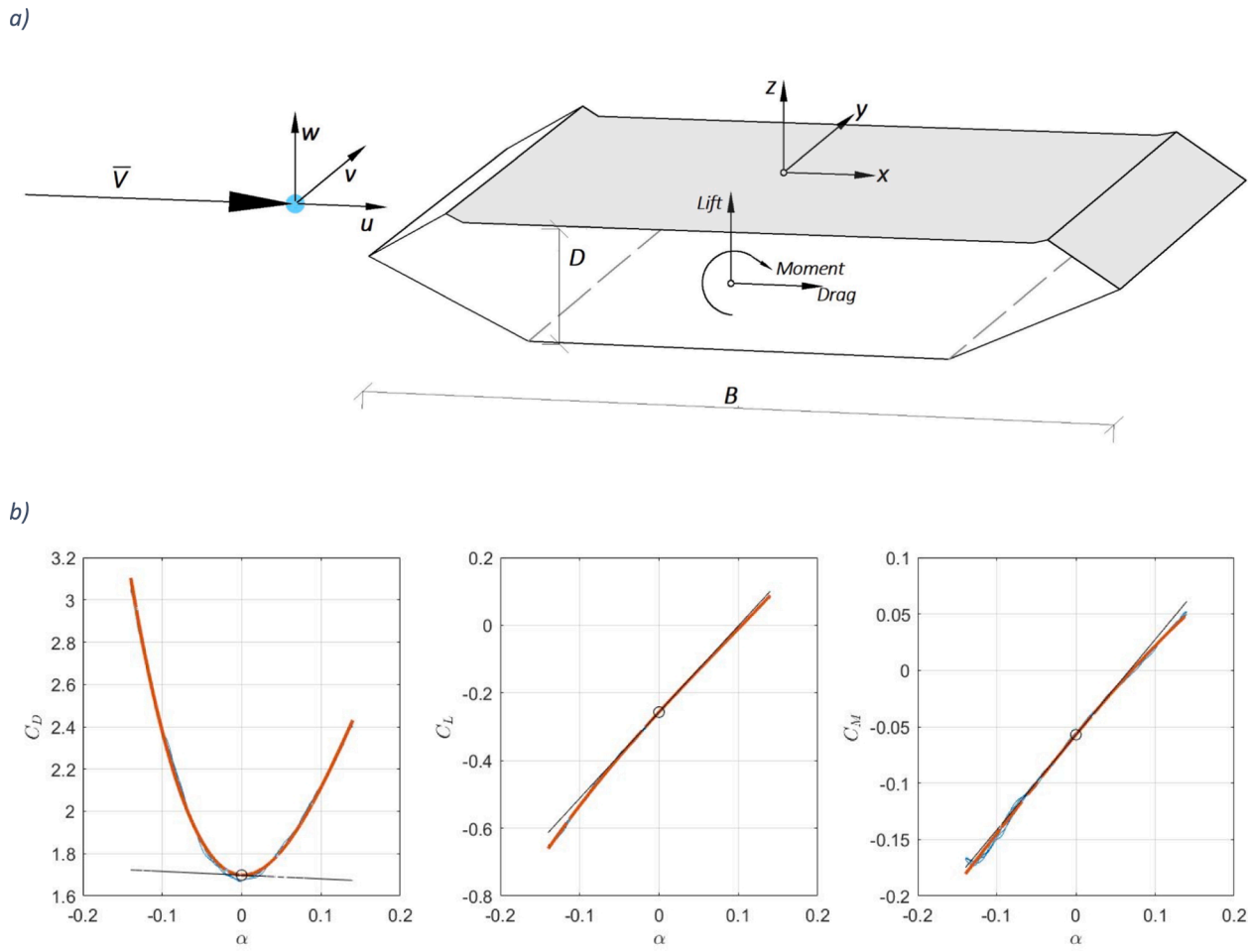

Fig. 7. a) Axis of static coefficients and buffeting actions, and b) static coefficients linearized with respect to the angle of attack α in radians: from left to right: drag, lift and moment force coefficients. The blue line shows the test measurements, the red line represents a polynomial fit to the data, and the black line is the first-order linearization around zero degrees.

Table 8
Load coefficients obtained from wind tunnel testing.

Load Coefficients	$\overline{C}_D$	$C_D^{'}$	$\overline{C}_L$	$C_L^{'}$	$\overline{C}_M$	$C_M^{'}$
Values	1.698	0.176	−0.257	2.549	−0.057	0.844

variability in the wind's turbulence field, which is accounted for in the ECM. The table shows that the maximum buffeting responses occur at wind states with lower mean wind speeds and higher turbulence intensities than those in the current design guidelines. This result is also in accordance with the results of the ECM on the Hardanger Bridge [14].

5.2. Extreme buffeting response with long-term methods

The extreme buffeting response in long-span bridges has not been estimated previously with full long-term analysis based on ISMC simulation. Therefore, the framework was tested and compared with the available formulations tested in sections 2.2.1 and 2.2.2. This section explains the settings used in the analysis. To simplify the responses' graphical interpretation, the uncertainties in the wind field were considered in terms of two variables: the mean wind speed and the vertical turbulence intensity. The vertical turbulence intensity was chosen over the along-wind component because the former strongly influences SM1 and SM3, whereas the latter mainly influences SM2. The remaining wind turbulence parameters were taken as fixed numbers obtained from the most likely value from the marginal distribution conditional on the mean wind speed.

5.2.1. Extreme buffeting response according to the inverse first-order reliability method (IFORM)

This section reports the settings and results of the long-term framework based on the IFORM. For a design *RP* of 100 years, the reliability index β_{RP} is 5.0785. Then, the initial point of the IFORM algorithm was set as $\{u1, u2, u3\}_0 = \{0,\ 0, \beta_{RP}\}$. Since the Rosenblatt transformation rule depends on the order of transformation, the mean wind speed was chosen as the first variable to transform (Appendix A).

Fig. 12 shows the IFORM procedure, and Table 13 summarizes the results. The mean wind speeds (V_{100}) reported by Table 13 are lower than the mean wind speed of the short-term methodology from Table 9. This demonstrates that the design condition may not necessarily be the extreme mean wind speed but rather wind states with slightly lower mean wind speeds but a higher influence on the turbulence parameters. In Fig. 12, the left-hand side presents the iterations in the standard normal space, while the right-hand side presents the contours in the wind variable space. The colormap in the figure represents the extreme response for each wind state. In the figure, the design point (represented with a star) is not at the tip of the contour, confirming that the design wind state is not precisely at the maximum mean wind speed. This behaviour is more evident in SM1 and SM3 than in SM2 because the latter is less affected by the vertical turbulence intensity I_w. Finally, it is important to note that the method requires more executions of buffeting analysis than the number of iteration points because the optimization procedure needs to compute the gradients of the limit function with

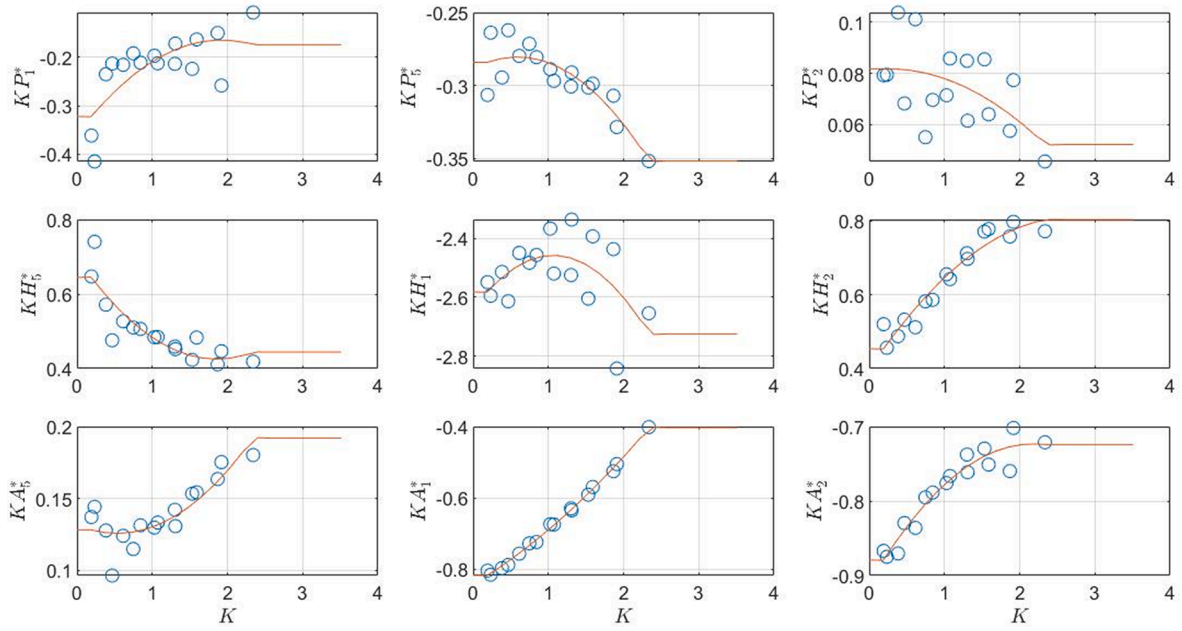

Fig. 8. Dimensionless aerodynamic derivatives related to aeroelastic stiffness as a function of the reduced frequency K: The scattered points are the results of experiments, and the continuous red lines are the fitted functions.

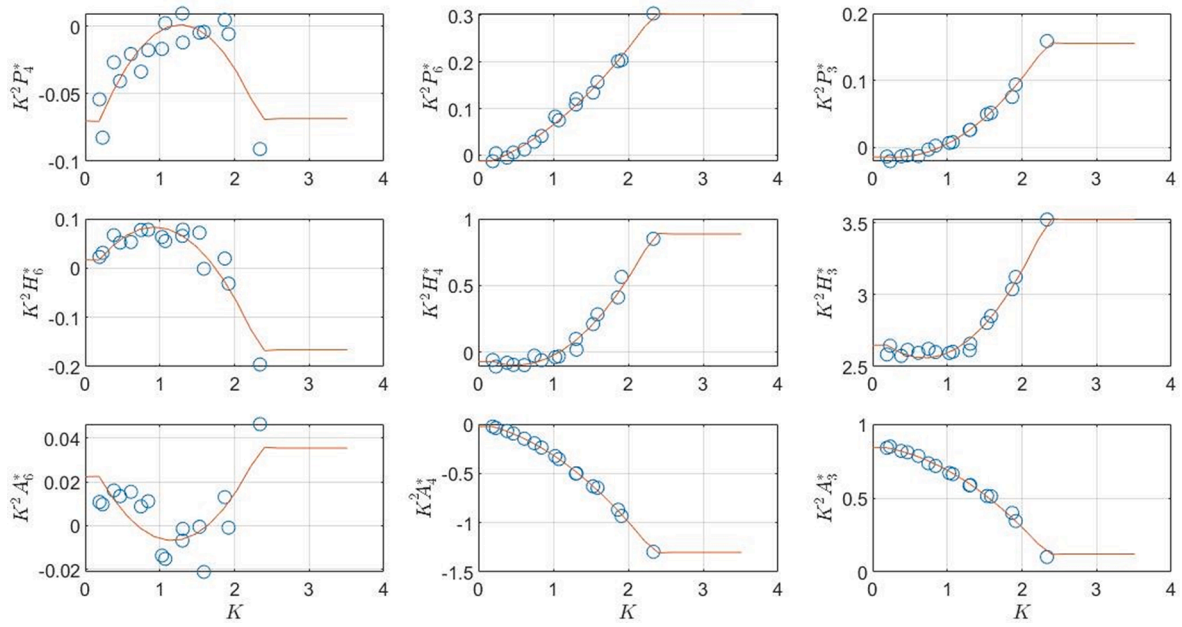

Fig. 9. Dimensionless aerodynamic derivatives related to aeroelastic damping as a function of the reduced frequency K: The scattered points are the results from experiments, and the continuous red lines are the fitted functions.

Table 9
Reference values from the mean wind speed and turbulence parameters.

V_{100}	I_u	I_w	A_u	A_w	K_u	K_w
42.1	0.078	0.038	12.08	5.33	10	8

respect to every u variable.

5.2.2. *Extreme buffeting response using the exact formulation*

The full long-term framework based on the numerical integration of Eq. (6) converges to an exact solution and was therefore taken as the control method for accuracy evaluation. This section explains the settings of the framework. The integration grid was set with 100 points for the mean wind speed and 50 points for the turbulence intensity. The integration domain for the mean wind speed was set from 5 to 60 m/s to avoid the flutter instability region, whereas the turbulence intensity was discretized from 0.005 to 0.25.

Fig. 13 shows the contours of the standard deviation of the internal moments. The contours are placed over a colormap of the normalized contribution of the wind states to the full long-term buffeting response. The points from the integration grid are not dense enough to draw an appropriate colormap. Therefore, only for the purposes of drawing the colormap was the grid further densified with an artificial neural network

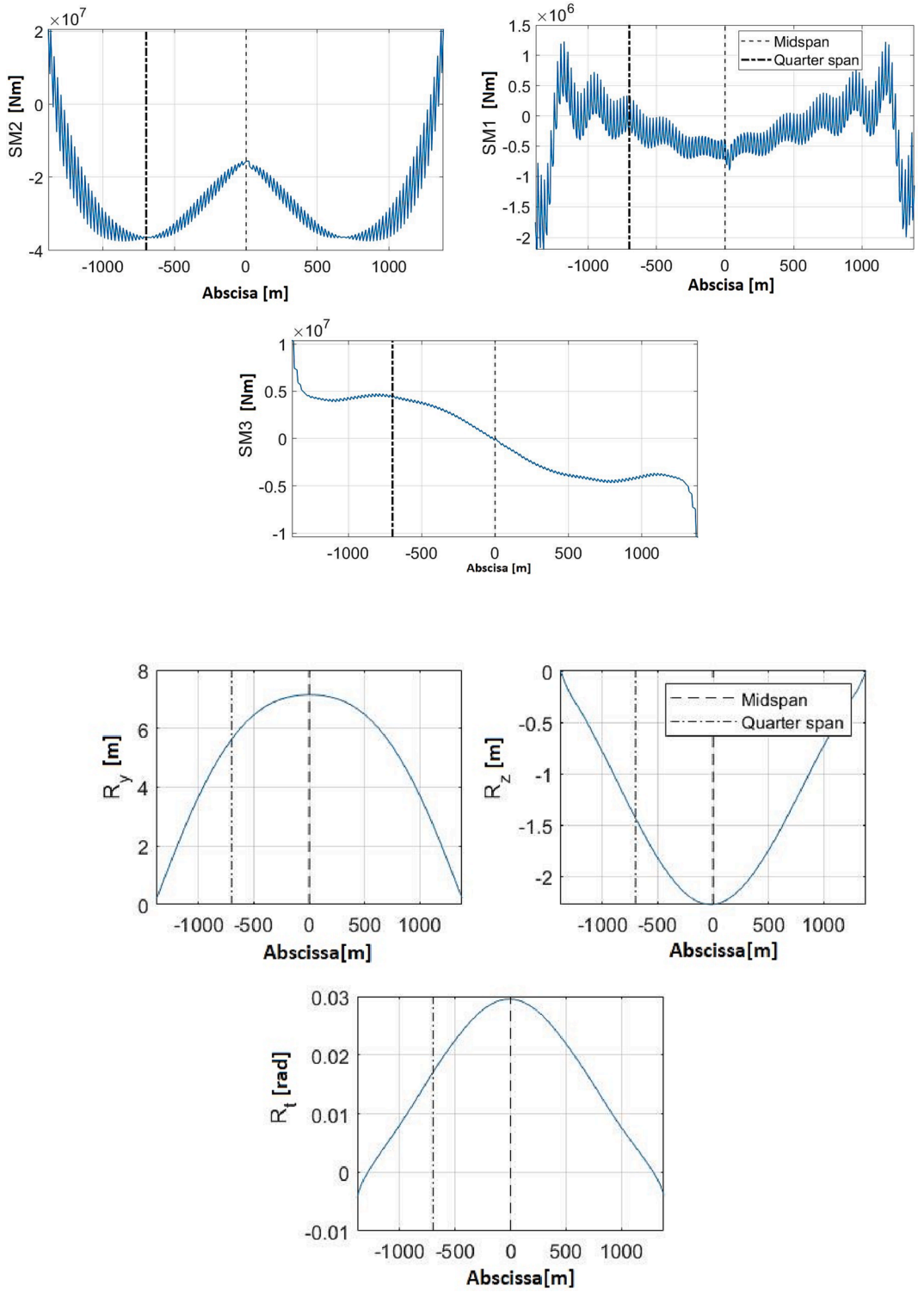

Fig. 10. Mean structural response along the girder for wind states with $RP = 100$ years.

surrogate model used to simulate the buffeting response, similar to that of [62]. The model was trained using the Statistics and Machine Learning tool box in MATLAB [67]. Seventy-five percent of the wind conditions used in the integration grid were for training and validation, whereas 25 % were used for testing, and the data points were randomized. The accuracy of the model in terms of the mean absolute percent error (MAPE) was above 99.7 %. The dashed line in the corresponding figures corresponds to the environmental contour line.

Fig. 13 also shows the results from the IFORM, the short-term method, and the ECM. The response according to the short-term method coincides with the contour tip, while that for the ECM coincides with the point in the contour line, closer to the centre of the coloured region. The solution from the IFORM is located inside the contour line and is larger than the response from the ECM. These two features are attributed to the fact that the IFORM, in contrast to the ECM, considers the response as a stochastic variable. Table 14 reports the extreme buffeting response from the exact formulation.

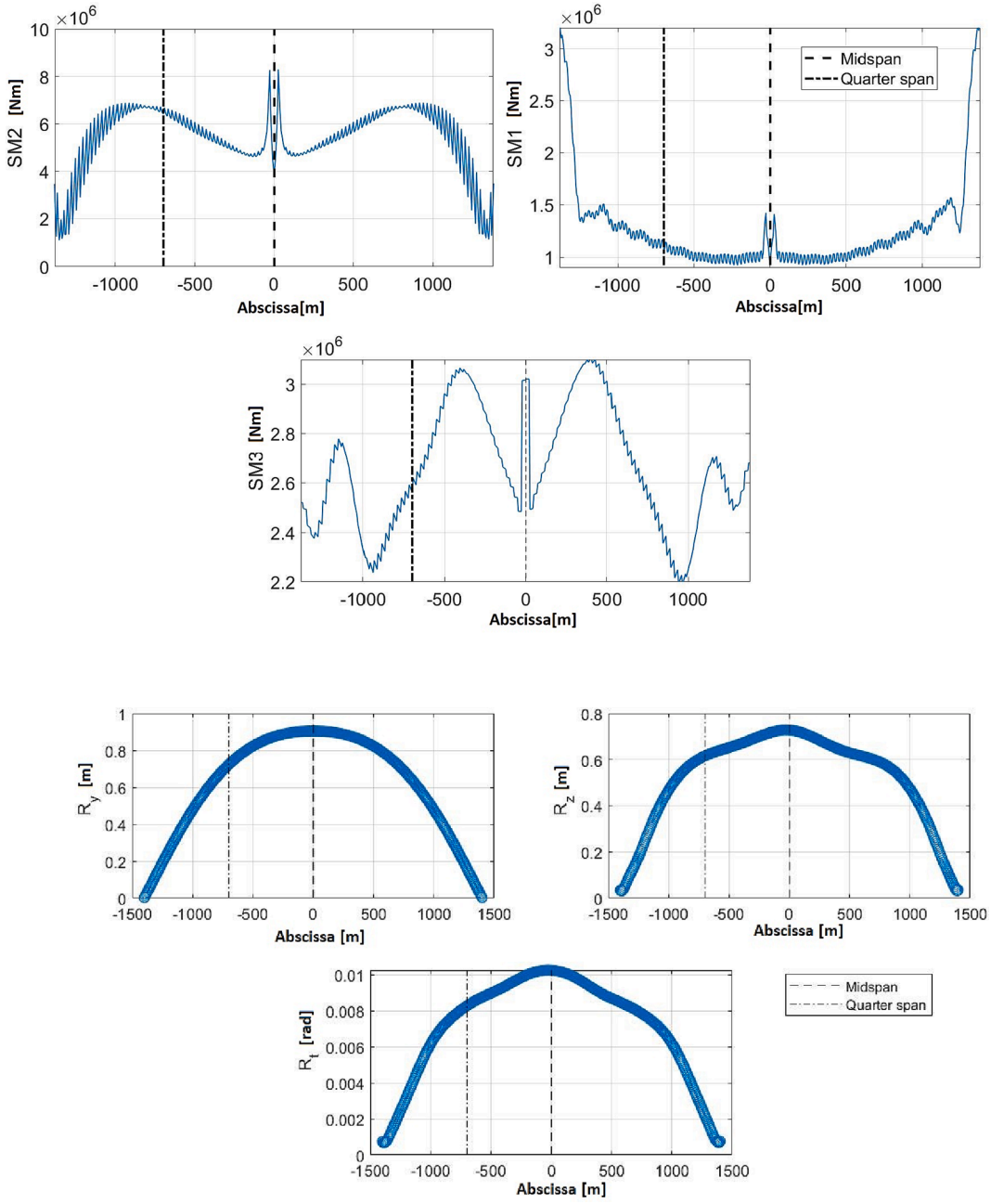

Fig. 11. Standard deviation of structural responses along the girder for wind states with $RP = 100$ years.

Table 10
Structural response statistics.

RP	$SM1$[Nm]	$SM2$[Nm]	$SM3$[Nm]	R_y[m]	R_z[m]	R_t[rad]
μ_R	−1.77e + 05	−3.66e + 07	4.18e + 06	5.638	−1.408	0.017
σ_R	1.09e + 06	6.41e + 06	2.56e + 06	0.722	0.613	0.0082

Table 11
Extreme buffeting response from the short-term response method.

R^{ST}_{SM1}[Nm]	R^{ST}_{SM2}[Nm]	R^{ST}_{SM3}[Nm]	R^{ST}_{y}[m]	R^{ST}_{z}[m]	R^{ST}_{t}[rad]
3.66e + 06	1.98e + 07	8.12e + 06	1.895	1.779	0.026

Table 12
Extreme buffeting response with the ECM.

	V[m/s]	I_w [−]	R^{ST}_{SM}[Nm]
SM1	39.88	0.054	4.56e + 06
SM2	42.57	0.043	2.10e + 07
SM3	40.26	0.053	9.84e + 06

5.2.3. *Extreme buffeting response according to ISMC simulation*

The settings of the proposed framework based on ISMC simulation are reported in this section. As explained in section 2.3, the sampling function has a multivariate uniform distribution that ensures that the generated wind states within the domain of the response prediction model are accurate. The distribution bounds are reported in Table 15. The simulations were generated by adding batches of 10 samples at a time and then estimating the extreme response. This was repeated until

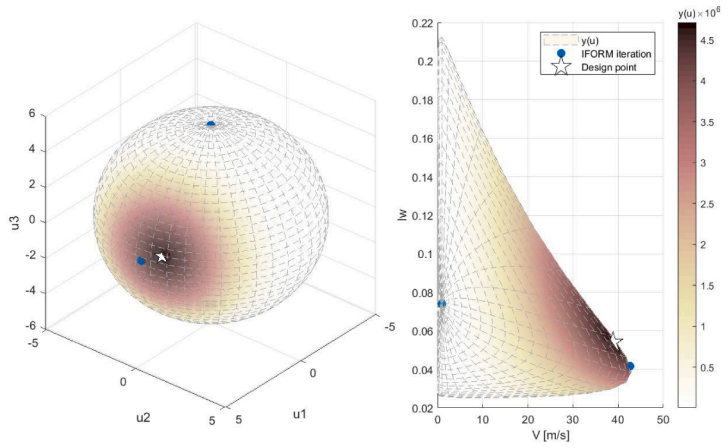

a) SM1. Left: isometric view of the extreme response in u-space; right: projection in the V-I_w plane.

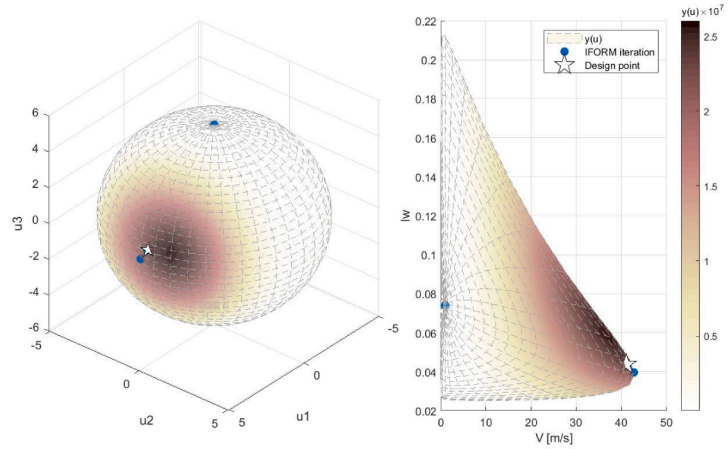

b) SM2. Left: isometric view of the extreme response in u-space; right: projection in the V-I_w plane.

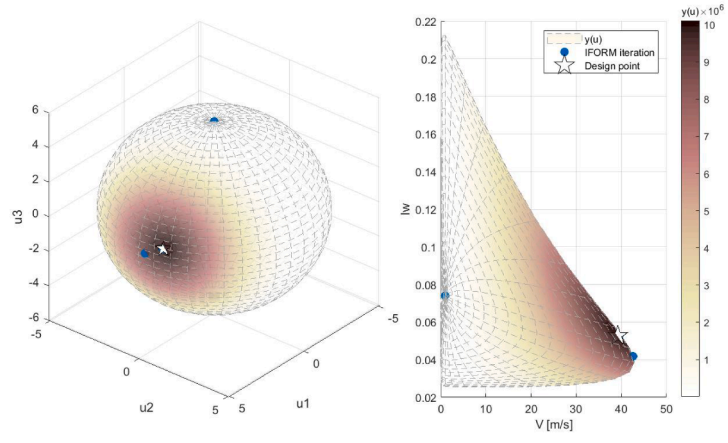

c) SM3. Left: isometric view of the extreme response in u-space; right: projection in the V-I_w plane.

Fig. 12. Graphical solution of the IFORM approximation.

Table 13
Results of analysis with the IFORM.

	$[u_1 u_2 u_3]_{design}$			*Simulations*	*Iterations*	V_{100} [m/s]	I_w [−]	R_{SM}^{100} [Nm]
SM1	4.82	1.39	0.78	36	6	38.47	0.05	4.63e + 06
SM2	4.97	0.46	0.91	36	6	41.08	0.043	2.18e + 07
SM3	4.84	1.27	0.80	29	5	38.94	0.053	1.01e + 07

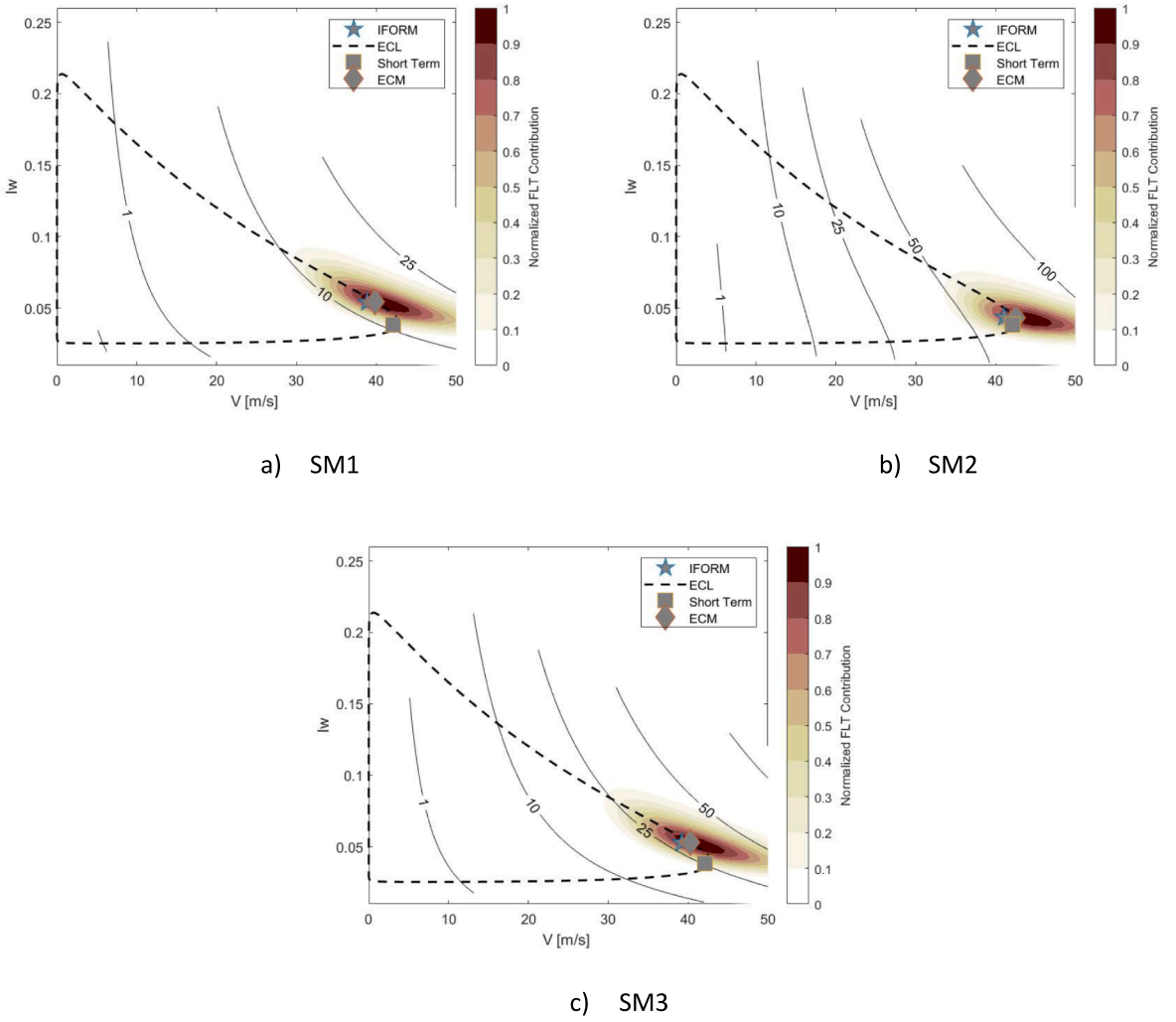

Fig. 13. Normalized contribution to the extreme buffeting response for a 100-year return period.

Table 14
Extreme buffeting response with the exact full long-term method.

R_{SM1}^{LT} [Nm]	R_{SM2}^{LT} [Nm]	R_{SM3}^{LT} [Nm]	R_y^{LT} [m]	R_z^{LT} [m]	R_t^{LT} [rad]
5.22e + 06	2.39e + 07	1.17e + 07	2.231	2.463	0.035

Table 15
Settings of the ISMC framework.

Variable	Lower limit (a)	Upper limit (b)
u_1	3.94	6
u_2	−2.53	3.46

the stopping criterion for convergence was met, which was defined as a less than 0.3 % change in the estimated extreme response for 3 subsequent batches.

Fig. 14 shows the convergence plots, while Table 16 reports the converged values of ISMC and the required number of simulations. Fig. 15 shows the simulations over the colormap of the normalized contribution to the full long-term response. The figure shows the distribution of the simulations, which are located in the region that contributes most to the full long-term response and is also outside the flutter instability region.

5.3. Response comparison

In what follows, the predicted extreme responses obtained from the different frameworks are compared to the exact formulation of the full long-term methodology. Table 17 summarizes the design buffeting response of the Sulafjord Bridge from the different methodologies. The

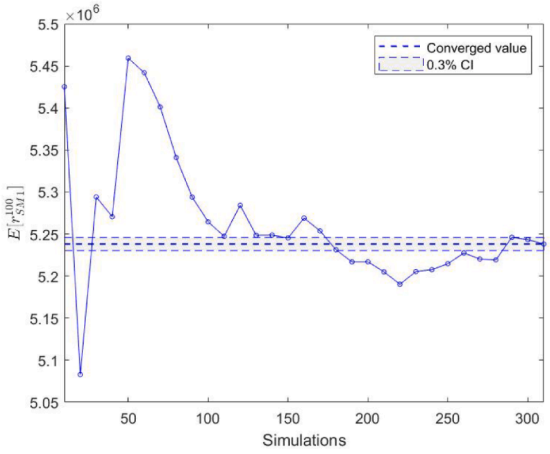

a) Convergence plot of the extreme value of SM1 from the ISMC results

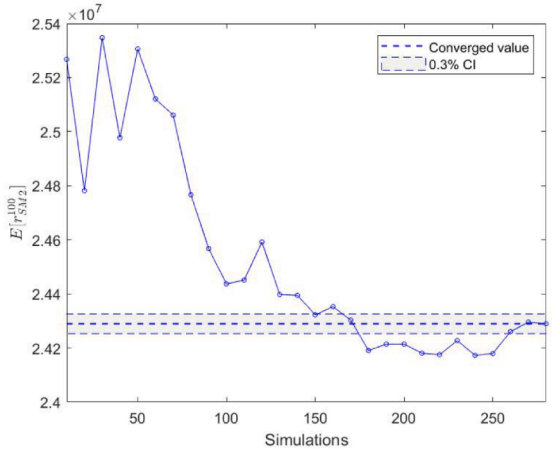

b) Convergence plot of the extreme value of SM2 from the ISMC results

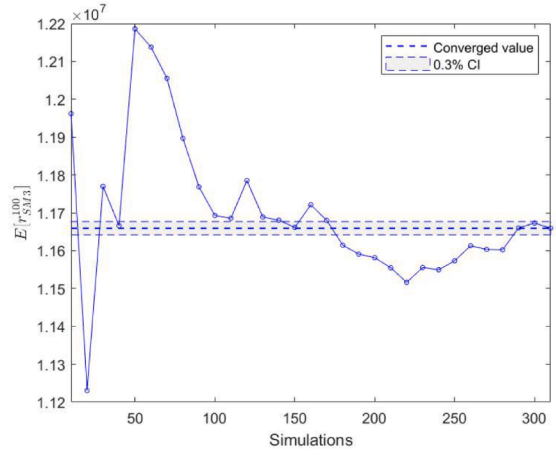

c) Convergence plot of the extreme value of SM3 from the ISMC results

Fig. 14. Convergence plot of the ISMC simulations.

percentages in the table represent the ratios between the response estimations and the exact response. The results of Table 17 show that the difference between the full long-term and short-term methods is between 25 and 30 % for SM1, SM3, R_t and R_z while 13 to 18 % for R_y and SM2. The estimations from the ECM and IFORM of the internal forces have similar trends, with a difference of 12 % with respect to the exact formulation. The difference between the two approaches is less than 4 % and can be attributed to the uncertainty in the response that is considered in the IFORM but not in the ECM. Nevertheless, as the IFORM converges to an approximate solution, the difference of 12 % with respect to the exact method is not negligible for structural design purposes and does not seem to give any more insight than the ECM, although the IFORM is a more computationally demanding framework.

The comparison provides insight into the accuracy of the framework based on the ISMC approach. Fig. 16 shows a comparison of the CDF of the extreme buffeting response from the ISMC framework and the exact formulation in addition to the reported values of Table 17. The estimations from both frameworks are similar, with reported differences of 0.19 to 4.43 %. Better results could be obtained with an optimization of the distribution from Eq. (14); however, such an analysis is outside the scope of this paper.

Table 16
Converged extreme responses from the ISMC approach.

	*SM*1[Nm]	*SM*2[Nm]	*SM*3[Nm]	$R_y[m]$	$R_z[m]$	*R*[rad]
R_{SMi}^{LT}	5.23e + 06	2.43e + 07	1.17e + 07	2.252	2.498	0.036
N_{sim}	310	280	310	280	250	280

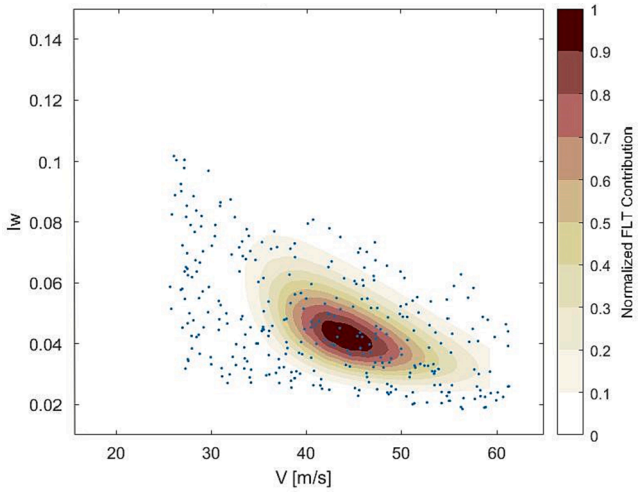

Fig. 15. ISMC simulation results.

Table 17
Extreme buffeting responses from different frameworks and the relative values compared to the exact formulation.

Method	R_{SM1} [Nm]		R_{SM2} [Nm]		R_{SM3} [Nm]	
Exact formulation	5.22E + 06	100.00 %	2.39E + 07	100.00 %	1.17E + 07	100.00 %
Short-term	3.66E + 06	70.11 %	1.98E + 07	82.85 %	8.12E + 06	69.40 %
ECM	4.56E + 06	87.36 %	2.10E + 07	87.87 %	9.84E + 06	84.10 %
IFORM	4.63E + 06	88.70 %	2.18E + 07	91.21 %	1.01E + 07	86.32 %
ISMC	5.23E + 06	100.19 %	2.43E + 07	101.6 %	1.17E + 07	95.57 %

Method	R_y[m]		R_z[m]		R_t[*rad*]	
Exact formulation	2.231	100%	2.463	100.00%	0.035	100.00%
Short-term	1.895	84.93%	1.779	72.22%	0.026	74.28%
ISMC	2.252	99.05%	2.498	98.57%	0.036	97.14%

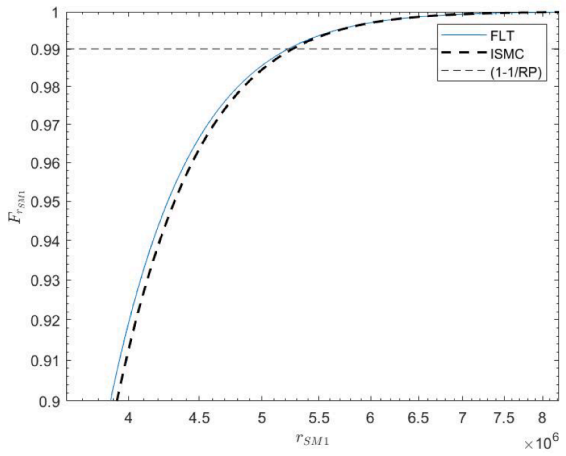

a) SM1

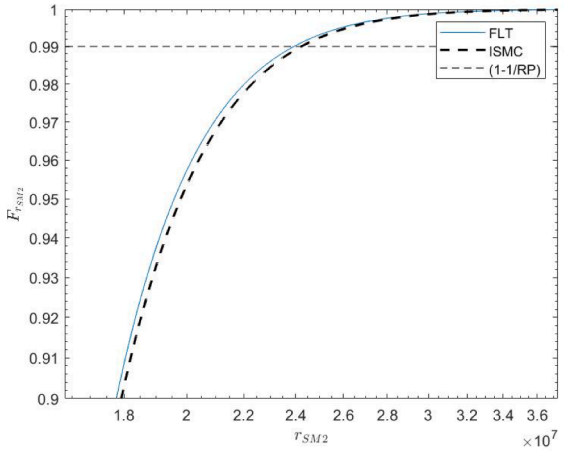

b) SM2

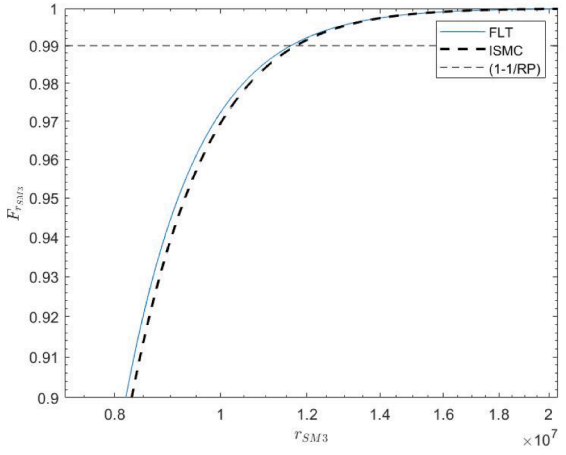

c) SM3

Fig. 16. Comparison of the CDF of the yearly extreme buffeting response from the ISMC approach and the exact formulation.

5.4. Long-term extreme buffeting response considering uncertainties from multiple wind variables

The accuracy of the proposed framework based on the ISMC approach was verified in the previous section. Nevertheless, the IFORM framework was found to be more computationally efficient than ISMC despite converging to an approximate solution. This section expands the investigation of the extreme buffeting response of the Sulafjord Bridge by considering uncertainties in multiple wind turbulence parameters and discusses the balance between the computational demand and accuracy of the two frameworks.

Two additional scenarios were considered to verify the effect of the wind turbulence parameters. First, a long-term analysis was carried out considering uncertainties in the mean wind speed (V) and the two turbulence intensity components (I_u and I_w). Then, the analysis was repeated with the addition of uncertainties from spectral parameters (A_u and A_w) and decay coefficients (K_u and K_w). Both analyses were included in the previous scenario considering the mean wind speed and the vertical turbulence component.

The settings of the IFORM and ISMC frameworks were as described in section 5.2. The solution using the IFORM is reported in Table 18. Fig. 17 shows the convergence plot of the ISMC simulations. The lines in each subfigure show stabilization with an increasing number of simulations. Therefore, the convergence rate does not seem to be drastically affected by the number of uncertainties introduced. The converged values are reported in Fig. 18 and Table 19.

The results show that the variability in SM1 and SM3 is correctly captured by considering uncertainties in the mean wind speed and the vertical turbulence intensity since no significant variation is added when other parameters are considered. On the other hand, the variability SM2 seems to be more sensitive to the wind's turbulence field, as the estimation has a significant increase when the uncertainty in the along-wind turbulence is included and subsequently when uncertainties from the remaining wind turbulence parameters are included.

The difference between the IFORM and ISMC frameworks is reported in Table 20. The comparison shows that the difference decreases as more uncertain wind field parameters are considered. However, the difference of 13 % for SM3 is not negligible for an important structure such as a superlong bridge.

Regarding the computational demand, the framework based on the IFORM for the cases studied converges with fewer simulations than ISMC. The left-hand side of Table 21 reports the number of simulations that each long-term framework required to complete the estimations of this study. However, for practical engineering applications, extreme response estimations should be carried out at different critical points along the bridge span. Therefore, the right-hand side of Table 21 reports an estimate of the number of simulations required if the investigations are carried out at three different locations along the bridge.

In this study, the same computing machine was used for all analyses (Intel core i7-8650U @1.90 GHz with 16 GB RAM), the execution time of multimodal buffeting response estimation was approximately 24 *sec*. Table 21 also reports an estimated execution time for the analysis case $W = \{V, I_u, I_w, A_u, A_w, K_u, K_w\}$. The number of simulations required considering all the uncertainties using the ISMC framework is half the number required for the framework based on the IFORM. Because of the optimization algorithm, the IFORM analysis can target only one response at a time and should therefore be repeated for each response metric at each location. Conversely, the framework based on the ISMC

Table 18
Extreme response estimations of the IFORM framework.

	$\{V, I_w\}$	$\{V, I_u, I_w\}$	$\{V, I_u, I_w, A_u, A_w, K_u, K_w\}$
R^{LT}_{SM1} [Nm]	4.63e + 06	4.72e + 06	4.67e + 06
R^{LT}_{SM2} [Nm]	2.18e + 07	2.54e + 07	2.77e + 07
R^{LT}_{SM3} [Nm]	1.00e + 07	1.01e + 07	1.02e + 07

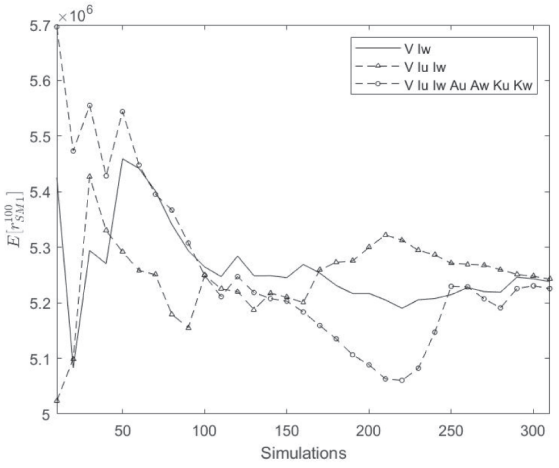

a) SM1

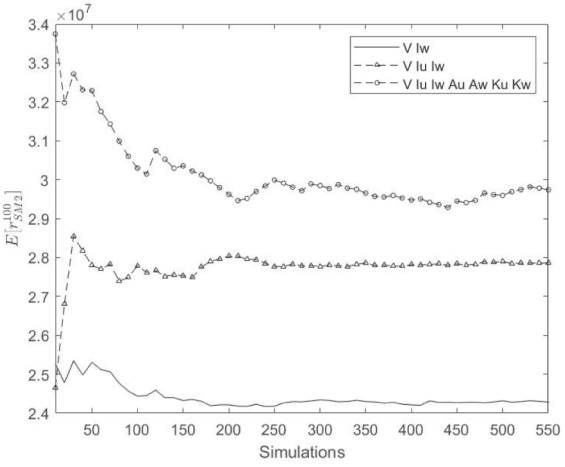

b) SM2

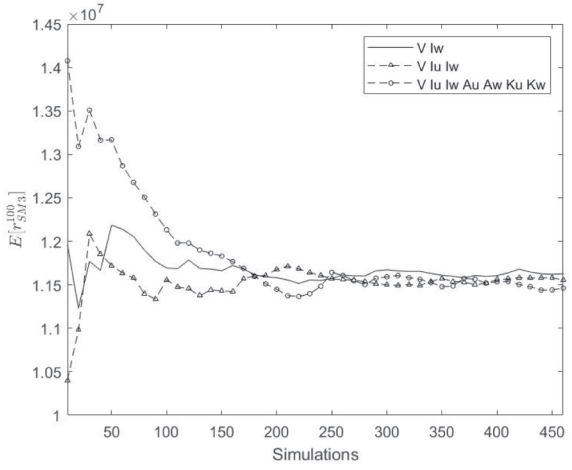

c) SM3

Fig. 17. Convergence plot of the ISMC extreme response considering different uncertainties.

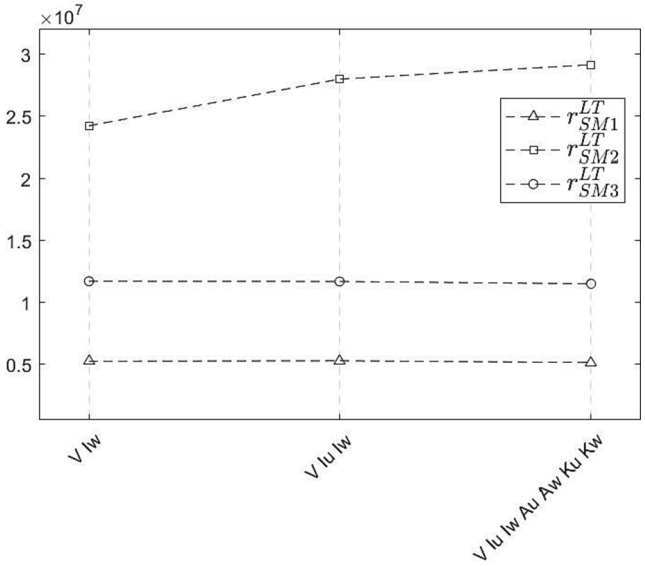

Fig. 18. Converged values of the extreme responses of ISMC simulations for different uncertainties.

Table 19
Converged values of the extreme response for different uncertainties using ISMC.

	$\{V, I_w\}$	$\{V, I_u, I_w\}$	$\{V, I_u, I_w, A_u, A_w, K_u, K_w\}$
R_{SM1}^{LT} [Nm]	5.23e + 06	5.30e + 06	5.15e + 06
R_{SM2}^{LT} [Nm]	2.43e + 07	2.80e + 07	2.91e + 07
R_{SM3}^{LT} [Nm]	1.17e + 07	1.17e + 07	1.15e + 07

Table 20
Difference in the extreme buffeting response between the IFORM and ISMC frameworks.

	$\{V, I_w\}$	$\{V, I_u, I_w\}$	$\{V, I_u, I_w, A_u, A_w, K_u, K_w\}$
R_{SM1}^{LT}	14 %	12 %	10 %
R_{SM2}^{LT}	11 %	10 %	5 %
R_{SM3}^{LT}	17 %	16 %	13 %

approach can estimate every response metric required for each simulation and thus does not require repetition. Therefore, the proposed long-term framework based on the ISMC approach is both more robust and computationally more efficient than the framework based on the IFORM.

6. Conclusion

In this paper, the extreme buffeting response of a proposed superlong bridge (L = 2800 m) was investigated with the proposed long-term framework based on the ISMC approach, considering uncertainties from multiple wind variables. The response features were compared with estimations from other frameworks, such as the short-term method (the basis of the current design guidelines), the ECM, the exact full long-term formulation and the framework based on the IFORM. The difference between the short-term method and the full long-term method was 18 % to 30 %. This result accords with previous studies of the Hardanger Bridge (a heavily monitored bridge; L = 1310 m), showing that ignoring the variability in the wind turbulence field and the probabilistic behaviour of the buffeting response may lead to underestimations of the extreme response in long-span bridges. The difference between the estimations from the ECM and the full long-term method was approximately 12 %. Although the ECM does not consider the variability in the buffeting response, it accounts for the stochastic behaviour of the wind

Table 21
Buffeting analysis required for 1 location (left) and 3 locations (right), and the estimated execution time for.. $W = \{V, I_u, I_w, A_u, A_w, K_u, K_w\}$

	$\{V, I_w\}$	$\{V, I_u, I_w\}$	$\{V, I_u, I_w, A_u, A_w, K_u, K_w\}$	Execution time [*sec*]	$\{V, I_w\}$	$\{V, I_u, I_w\}$	$\{V, I_u, I_w, A_u, A_w, K_u, K_w\}$	Execution time [*sec*]
FLT	5000	250 k	+150G	–	5000	250 k	+150G	–
IFORM	101	111	343	8232	303	333	1029	24,696
ISMC	310	280	550	13,200	310	280	550	13,200

turbulence parameters, providing an increased degree of reliability compared to the current design guidelines by using only the information that is typically available for long-span bridge designs. The ECM showed similar behaviour to the IFORM, with a difference of less than 4 %. Nevertheless, the latter method is computationally more demanding than the former, and the difference in accuracy is not very remarkable. Further research on the ECM should be conducted to verify the feasibility of the framework for practical engineering applications.

The similarity between the proposed framework based on the ISMC approach and the exact formulation was remarkable. Since the simulations were generated in the region that contributed most to the full long-term response, the difference between the two methods was less than 1.6 %, showing the good quality of the proposed framework. However, the selection of the sampling distribution parameters in this study was made by an engineering criterion. Further research should be conducted to define the optimal location and shape of the sampling function.

Regarding the computational effort for the case considered in the study, the framework based on the IFORM required fewer simulations than that based on the ISMC approach. Nevertheless, if response investigations for practical engineering applications are required in at least 3 locations along the bridge, the number of simulations required by the proposed framework is half that required by the IFORM. Therefore, the proposed ISMC framework is both more robust and more computationally efficient than the IFORM framework.

CRediT authorship contribution statement

Dario Fernandez Castellon: Writing – original draft, Software, Methodology, Formal analysis. **Aksel Fenerci:** Writing – review & editing, Data curation, Investigation. **Ole Øiseth:** Conceptualization, Writing – review & editing, Supervision, Project administration. **Øyvind Wiig Petersen:** Writing – review & editing.

Declaration of Competing Interest

The authors declare that they have no known competing financial interests or personal relationships that could have appeared to influence the work reported in this paper.

Data availability

Data will be made available on request.

Acknowledgements

This work was financially supported by the Norwegian Public Road Administration (NPRA) as a part of the E-39 Coastal highway project.

Appendix A. Variable transformation rules

The Weibull-distributed mean wind speed was transformed with the Rosenblatt transform [50], while the correlated lognormal distributed turbulence parameters were transformed with a linear transform.

The Rosenblatt transformation works by obtaining the joint CDF from the product of the marginals:

$$F_{x1x2..xn}(x_1, x_2, \cdots, x_n) = F_{x1}(x_1)F_{x2}(x_2|x_1)\cdots F_{xn}(x_n|x_{n-1}\cdots x\_1) \tag{18}$$

Then, the variables are transformed by considering the conditional distributions individually. The mean wind speed was chosen as the first variable, as it is considered the most important variable for determining the buffeting response of long-span bridges [62]. The mean wind speed was transformed as follows:

$$F_V(V) = \Phi(u_1) \leftrightarrow V = F_V^{-1}[\Phi(u_1)] \tag{19}$$

When the stochastic variables are correlated and normally distributed, the linear transformation rule can be applied.

$$\boldsymbol{U} = \boldsymbol{A}(\boldsymbol{X} - \boldsymbol{M}_X) \leftrightarrow \boldsymbol{X} = \boldsymbol{A}^{-1}\boldsymbol{U} + \boldsymbol{M}_X$$

$$\boldsymbol{M}_X = [\mu_{x_1}\mu_{x_2}, \cdots, \mu_{x_n}]^T \tag{20}$$

where A is a triangular matrix that can be found using the Cholesky decomposition of the covariance matrix $\boldsymbol{C}_{XX}$, which is Hermitian and positive definite:

$$\boldsymbol{C}_{XX} = \boldsymbol{A}^{-1}\boldsymbol{A}^{-T} \tag{21}$$

with.

$$\boldsymbol{C}_{XX} = \begin{bmatrix} \sigma_{x_1}^2 & \rho_{12}\sigma_{x_1}\sigma_{x_2} & \cdots & \rho_{1n}\sigma_{x_1}\sigma_{x_n} \\ \rho_{21}\sigma_{x_1}\sigma_{x_2} & \sigma_{x_2}^2 & \cdots & \rho_{2n}\sigma_{x_2}\sigma_{x_n} \\ \vdots & \vdots & \ddots & \vdots \\ \rho_{n1}\sigma_{x_1}\sigma_{x_n} & \rho_{n2}\sigma_{x_2}\sigma_{x_n} & \cdots & \sigma_{x_n}^2 \end{bmatrix} \tag{22}$$

Then, for the case in which the stochastic variables are correlated and lognormally distributed, the same transformation rule procedure applies, and the lognormal variables can be found as follows:

$$\boldsymbol{X} = exp(\boldsymbol{A}^{-1}\boldsymbol{U} + \boldsymbol{M}_X) \tag{23}$$

The full set of turbulence parameters conditional on the mean wind speed are transformed in a single operation using the linear transformation rule for the case of the lognormally distributed variables from Eq. (23).

$$F_{I_u,I_v,I_w,A_u,A_v,A_w|V}(I_u, I_v, I_w, A_u, A_v, A_w|V) = \Phi(u_2, u_3, u_4, u_5, u_6, u_7) \tag{24}$$

References

[1] Fenerci A, Øiseth O, Rønnquist A. Long-term monitoring of wind field characteristics and dynamic response of a long-span suspension bridge in complex terrain. Eng Struct 2017;147:269–84. https://doi.org/10.1016/j.engstruct.2017.05.070.

[2] Lystad TM, Fenerci A, Øiseth O. Evaluation of mast measurements and wind tunnel terrain models to describe spatially variable wind field characteristics for long-span bridge design. J Wind Eng Ind Aerodyn 2018;179(June):558–73. https://doi.org/10.1016/j.jweia.2018.06.021.

[3] Fenerci A. Full-scale investigation of the effects of wind turbulence characteristics on dynamic behavior of long-span cablesupported bridges in complex terrain. NTNU 2018.

[4] Meng X, et al. Design and implementation of a new system for large bridge monitoring—geoshm. Sensors (Switzerland) 2018;18(3). https://doi.org/10.3390/s18030775.

[5] Song J-L, Li J-W, Flay R. Field measurements and wind tunnel investigation of wind characteristics at a bridge site in a Y-shaped valley. J Wind Eng Ind Aerodyn Jul. 2020;202:104199. https://doi.org/10.1016/j.jweia.2020.104199.

[6] Wang H, Tao T, Gao Y, Xu F. Measurement of Wind Effects on a Kilometer-Level Cable-Stayed Bridge during Typhoon Haikui. J Struct Eng 2018;144(9):04018142. https://doi.org/10.1061/(asce)st.1943-541x.0002138.

[7] Fang C, Tang H, Li Y, Zhang J. Stochastic response of a cable-stayed bridge under non-stationary winds and waves using different surrogate models. Ocean Eng 2020;199(September). https://doi.org/10.1016/j.oceaneng.2020.106967. 2019, p. 106967.

[8] Zhang Y-M, Wang H, Mao J-X, Xu Z-D, Zhang Y-F. Probabilistic Framework with Bayesian Optimization for Predicting Typhoon-Induced Dynamic Responses of a Long-Span Bridge. J Struct Eng 2021;147(1):04020297. https://doi.org/10.1061/(asce)st.1943-541x.0002881.

[9] Cheynet E, Jakobsen JB, Snæbjörnsson J. Buffeting response of a suspension bridge in complex terrain. Eng Struct 2016;128:474–87. https://doi.org/10.1016/j.engstruct.2016.09.060.

[10] Midjiyawa Z, Cheynet E, Reuder J, Ágústsson H, Kvamsdal T. Potential and challenges of wind measurements using met-masts in complex topography for bridge design: Part I - Integral flow characteristics. J Wind Eng Ind Aerodyn 2020;211(October):2021. https://doi.org/10.1016/j.jweia.2021.104584.

[11] He X, Li H, Hu L, Wang H, Kareem A. Crosswind aerodynamic characteristics of a stationary interior railway carriage through a long-span truss-girder bridge. Eng Struct 2020;210(February):110350. https://doi.org/10.1016/j.engstruct.2020.110350.

[12] Kareem A. Numerical simulation of wind effects: A probabilistic perspective. J Wind Eng Ind Aerodyn 2008;96(10–11):1472–97. https://doi.org/10.1016/j.jweia.2008.02.048.

[13] Hu L, Xu Y-L, Huang W-F. Typhoon-induced non-stationary buffeting response of long-span bridges in complex terrain. Eng Struct 2013;57:406–15. https://doi.org/10.1016/j.engstruct.2013.09.044.

[14] Lystad TM, Fenerci A, Øiseth O. Buffeting response of long-span bridges considering uncertain turbulence parameters using the environmental contour method. Eng Struct 2020;213(March):110575. https://doi.org/10.1016/j.engstruct.2020.110575.

[15] CEN, Eurocode 1: Actions on structures - Part 1-4: General actions - Wind actions, vol. 1, no. 2005. 2004.

[16] Wang H, Zhang YM, Mao JX. Sparse Gaussian process regression for multi-step ahead forecasting of wind gusts combining numerical weather predictions and on-site measurements. J Wind Eng Ind Aerodyn 2022;220(October 2021):104873.

[17] Chen X. Analysis of Multimode Coupled Buffeting Response of Long-Span Bridges to Nonstationary Winds with Force Parameters from Stationary Wind. J Struct Eng 2015;141(4):04014131. https://doi.org/10.1061/(asce)st.1943-541x.0001078.

[18] Naess A. Technical note: On the long-term statistics of extremes. Appl Ocean Res 1984;6:227–8.

[19] Borgman LE. Probabilities for Highest Wave in Hurricane. J Waterw Harb Coast Eng Div 1973;99(2):185–207.

[20] Nordenström, "Methods for predicting long-termdistributions of wave loads and probability of failure for ships DnV report no. 69-21-S. Det Norske Veritas (Høvik)," 1969.

[21] Karmakar D, Bagbanci H, Guedes Soares C. Long-term extreme load prediction of spar and semisubmersible floating wind turbines using the environmental contour method. J Offshore Mech Arct Eng 2016;138(2):1–9. https://doi.org/10.1115/1.4032099.

[22] Giske FIG, Leira BJ, Øiseth O. Long-term extreme response analysis of marine structures using inverse SORM. J Offshore Mech Arct Eng 2018;140(5):1–7. https://doi.org/10.1115/1.4039718.

[23] Fedele F, Arena F. Long-term statistics and extreme waves of sea storms. J Phys Oceanogr 2010;40(5):1106–17. https://doi.org/10.1175/2009JPO4335.1.

[24] Xu Y, Øiseth O, Naess A, Moan T. Prediction of long-term extreme load effects due to wind for cable-supported bridges using time-domain simulations. Eng Struct 2017;148:239–53. https://doi.org/10.1016/j.engstruct.2017.06.051.

[25] Agarwal P, Manuel L. Simulation of offshore wind turbine response for long-term extreme load prediction. Eng Struct 2009;31(10):2236–46. https://doi.org/10.1016/j.engstruct.2009.04.002.

[26] Vanem E. and Huseby AB. "Combined long-term and short-term description of extreme ocean wave conditions by 3-dimensional environmental contours," in: Proceedings of the International Offshore and Polar Engineering Conference, 2018, vol. 2018-June, pp. 470–477.

[27] Moan T, Gao Z, Ayala-Uraga E. Uncertainty of wave-induced response of marine structures due to long-term variation of extratropical wave conditions. Mar struct 2005;18(4):359–82. https://doi.org/10.1016/j.marstruc.2005.11.001.

[28] Zhang Y, Beer M, Quek ST. Long-term performance assessment and design of offshore structures. Comput Struct 2015;154:101–15. https://doi.org/10.1016/j.compstruc.2015.02.029.

[29] Xu Y, Øiseth O, Moan T, Naess A. Prediction of long-term extreme load effects due to wave and wind actions for cable-supported bridges with floating pylons. Eng Struct 2018;172(June):321–33. https://doi.org/10.1016/j.engstruct.2018.06.023.

[30] Lystad TM, Fenerci A, Øiseth O. Long-term extreme buffeting response of cable-supported bridges with uncertain turbulence parameters. Eng Struct 2021;236(March). https://doi.org/10.1016/j.engstruct.2021.112126.

[31] Giske FIG, Leira BJ, Øiseth O. Full long-term extreme response analysis of marine structures using inverse FORM. Probabilistic Eng Mech 2017;50(October):1–8. https://doi.org/10.1016/j.probengmech.2017.10.007.

[32] Giske FIG, Kvåle KA, Leira BJ, Øiseth O. Long-term extreme response analysis of a long-span pontoon bridge. Mar struct 2018;58(November 2017):154–71. https://doi.org/10.1016/j.marstruc.2017.11.010.

[33] Moustapha M. and Sudret B. "Surrogate-assisted reliability-based design optimization: A survey and a new general framework," arXiv, 2019. pp. 2157–2176.

[34] Lystad TM. "Tor Martin Lystad Long-term extreme buffeting response investigations for long-span bridges considering uncertain turbulence parameters based on field measurements," no. March, 2021.

[35] Vázquez-Hernández AO, Ellwanger GB, Sagrilo LVS. Long-term response analysis of FPSO mooring systems. Appl Ocean Res 2011;33(4):375–83. https://doi.org/10.1016/j.apor.2011.05.003.

[36] Low YM, Huang X. Long-term extreme response analysis of offshore structures by combining importance sampling with subset simulation. Struct Saf 2017;69:79–95. https://doi.org/10.1016/j.strusafe.2017.08.001.

[37] Zhao Y, Dong S. Long-term extreme response analysis for semi-submersible platform mooring systems. Proc Inst Mech Eng Part M J Eng Marit Environ 2021;235(2):463–79. https://doi.org/10.1177/1475090220976515.

[38] Gao Y, Low YM. An efficient importance sampling method for long-term fatigue assessment of deepwater risers with time domain analysis. Probabilistic Eng Mech 2016;45:102–14. https://doi.org/10.1016/j.probengmech.2016.04.003.

[39] Melchers Robert E. and Beck AT. "Integration and Simulation Methods," Structural Reliability Analysis and Prediction Oct. 02, 2017, . pp. 63–93. doi: https://doi.org/10.1002/9781119266105.ch3.

[40] Sagrilo LVS, Naess A, Doria AS. On the long-term response of marine structures. Appl Ocean Res 2011;33(3):208–14. https://doi.org/10.1016/j.apor.2011.02.005.

[41] Castellon DF, Fenerci A, and Ole Ø. "Environmental contours for wind-resistant bridge design in complex terrain," J Wind Eng Ind Aerodyn, no. February, 2022, doi: 10.1016/j.jweia.2022.104943.

[42] Statens Vegvesen, Håndbok N400 Bruprosjektering. 2015.

[43] Rice SO. Mathematical Analysis of Random Noise. Bell Syst Tech J 1945;24(1):46–156. https://doi.org/10.1002/j.1538-7305.1945.tb00453.x.

[44] Davenport AG. Note on the Distribution of the Largest Value of a Random Function With Application To Gust Loading. Proc Inst Civ Eng 1964;28(2):187–96. https://doi.org/10.1680/iicep.1964.10112.

[48] Naess A, Moan T. Stochastic Dynamics of Marine Structures. Cambridge: Cambridge University Press; 2012.

[49] Winterstein SR, Ude TC, a Cornell C, Bjerager P. and Haver S. "Environmental Parameters for Extreme Response: Inverse Form with Omission Factors," Icossar-93, no. August, pp. 9–13, 1993.

[50] Rosenblatt M. Remarks on a Multivariate Transformation Author (s): Murray Rosenblatt Published by : Institute of Mathematical Statistics Stable URL : http://www.jstor.org/stable/2236692 REFERENCES Linked references are available on JSTOR for this article. Ann Math Stat 1952;23(3):470–2.

[51] Furevik BR, Agustsson H, Lauen Borg A, Midjiyawa Z, Nyhammer F, Gausen M. Meteorological observations in tall masts for the mapping of atmospheric flow in

Norwegian fjords. Earth Syst Sci Data 2020;12(4):3621–40. https://doi.org/10.5194/essd-12-3621-2020.
[52] Kjeller Vindteknikk, "Sulafjorden og Vartdalsfjorden , Møre og Romsdal Analyse av modellert vind , strøm og bølger for," 2018.
[53] Kjeller Vindteknikk, "Analysis of wind measurements from 6 masts at Sulafjorden," 2019.
[54] Norwegian Meteorological Institute, "observasjonsdata i SVV-E39-prosjektet," 2020. https://thredds.met.no/thredds/catalog/obs/mast-svv-e39/catalog.html.
[55] Statens Vegvesen, "E39 Sulafjorden Multispan suspension bridge om GBS Feasibility studies-Presentation." 2016, [Online]. Available: https://www.vegvesen.no/_attachment/1545452/binary/1135150?fast_title=16+Flerspenns+hengebru+på+fast+fundament+%28GBS%29.pdf.
[56] Kaimal JC, Wyngaard JC, Izumi Y, Coté OR. Spectral characteristics of surface-layer turbulence. Q J R Meteorol Soc 1972;98(417):563–89. https://doi.org/10.1002/qj.49709841707.
[57] Davenport AG. "Buffetting of a Suspension Bridge by Storm Winds," J Struct Div vol. 88, no. 3, 1962, doi: https://doi.org/10.1061/JSDEAG.0000773.
[58] Fenerci A, Øiseth O. Site-specific data-driven probabilistic wind field modeling for the wind-induced response prediction of cable-supported bridges. J Wind Eng Ind Aerodyn 2018;181(June):161–79. https://doi.org/10.1016/j.jweia.2018.09.002.
[59] Chen X, Matsumoto M. and Kareem A. "Aerodynamic coupling effects on flutter and buffeting of bridges," vol. 126, no. January, pp. 17–26, 2000.
[60] Katsuchi H, Jones NP, Scanlan RH, Akiyama H. Multi-mode flutter and buffeting analysis of the Akashi-Kaikyo bridge. J Wind Eng Ind Aerodyn 1998;77–78:431–41. https://doi.org/10.1016/S0167-6105(98)00162-7.
[61] Jain A, Jones NP, Scanlan RH. Coupled aeroelastic and aerodynamic response analysis of long-span bridges. J Wind Eng Ind Aerodyn 1996;60(1–3):69–80. https://doi.org/10.1016/0167-6105(96)00024-4.
[62] Castellon DF, Fenerci A, Øiseth O. A comparative study of wind-induced dynamic response models of long-span bridges using artificial neural networks, support vector regression and buffeting theory. J Wind Eng Ind Aerodyn 2021;209:104484. https://doi.org/10.1016/j.jweia.2020.104484.
[63] Dassault Systems, "Abaqus." .
[64] Møller RN, Krenk S, Svendsen MN. Damping system for long-span suspension bridges. Struct Control Heal Monit 2019;26(12):1–23. https://doi.org/10.1002/stc.2448.
[65] I. The Matworks, "Bayesopt." The Matworks Inc, 2016, [Online]. Available: https://se.mathworks.com/help/stats/bayesopt.html.
[66] Siedziako B, Øiseth O, Rønnquist A. An enhanced forced vibration rig for wind tunnel testing of bridge deck section models in arbitrary motion. J Wind Eng Ind Aerodyn 2017;164(December 2016):152–63. https://doi.org/10.1016/j.jweia.2017.02.011.
[67] I. The Matworks, "Statistics and Machine Learning ToolBox." https://se.mathworks.com/products/statistics.html.